NASA/CR–2012-217559

Design of a Slotted, Natural-Laminar-Flow Airfoil for Business-Jet Applications

Dan M. Somers
Airfoils, Incorporated, Port Matilda, Pennsylvania

July 2012

NASA STI Program . . . in Profile

Since its founding, NASA has been dedicated to the advancement of aeronautics and space science. The NASA scientific and technical information (STI) program plays a key part in helping NASA maintain this important role.

The NASA STI program operates under the auspices of the Agency Chief Information Officer. It collects, organizes, provides for archiving, and disseminates NASA's STI. The NASA STI program provides access to the NASA Aeronautics and Space Database and its public interface, the NASA Technical Report Server, thus providing one of the largest collections of aeronautical and space science STI in the world. Results are published in both non-NASA channels and by NASA in the NASA STI Report Series, which includes the following report types:

- TECHNICAL PUBLICATION. Reports of completed research or a major significant phase of research that present the results of NASA programs and include extensive data or theoretical analysis. Includes compilations of significant scientific and technical data and information deemed to be of continuing reference value. NASA counterpart of peer-reviewed formal professional papers, but having less stringent limitations on manuscript length and extent of graphic presentations.

- TECHNICAL MEMORANDUM. Scientific and technical findings that are preliminary or of specialized interest, e.g., quick release reports, working papers, and bibliographies that contain minimal annotation. Does not contain extensive analysis.

- CONTRACTOR REPORT. Scientific and technical findings by NASA-sponsored contractors and grantees.

- CONFERENCE PUBLICATION. Collected papers from scientific and technical conferences, symposia, seminars, or other meetings sponsored or co-sponsored by NASA.

- SPECIAL PUBLICATION. Scientific, technical, or historical information from NASA programs, projects, and missions, often concerned with subjects having substantial public interest.

- TECHNICAL TRANSLATION. English-language translations of foreign scientific and technical material pertinent to NASA's mission.

Specialized services also include creating custom thesauri, building customized databases, and organizing and publishing research results.

For more information about the NASA STI program, see the following:

- Access the NASA STI program home page at *http://www.sti.nasa.gov*

- E-mail your question via the Internet to help@sti.nasa.gov

- Fax your question to the NASA STI Help Desk at 443-757-5803

- Phone the NASA STI Help Desk at 443-757-5802

- Write to:
  NASA STI Help Desk
  NASA Center for AeroSpace Information
  7115 Standard Drive
  Hanover, MD 21076-1320

NASA/CR–2012-217559

Design of a Slotted, Natural-Laminar-Flow Airfoil for Business-Jet Applications

Dan M. Somers
Airfoils, Incorporated, Port Matilda, Pennsylvania

National Aeronautics and
Space Administration

Langley Research Center
Hampton, Virginia 23681-2199

Prepared for Langley Research Center
under Purchase Order NNL04AD45P

July 2012

Acknowledgments

This research was performed from February 1, 2004 to August 31, 2004 in response to NRA-03-LaRC-02.

Available from:

NASA Center for AeroSpace Information
7115 Standard Drive
Hanover, MD 21076-1320
443-757-5802

ABSTRACT

A 14-percent-thick, slotted, natural-laminar-flow airfoil, the S204, for light business-jet applications has been designed and analyzed theoretically. The two primary objectives of high maximum lift, relatively insensitive to roughness, and low profile drag have been achieved. The drag-divergence Mach number is predicted to be greater than 0.70.

INTRODUCTION

The wing profile drag is the largest contributor to the total aircraft drag at cruise conditions for most aircraft. The wing profile drag contributes about one third of the total drag for transport aircraft. As the aircraft size decreases from transport through commuter to business jets and other general-aviation (GA) aircraft and finally unmanned aerial vehicles (UAV's) and sailplanes, the percentage of the total aircraft drag due to the wing profile drag generally increases, primarily because the relative wing area increases, as shown in the following table.

Aircraft Type	$\frac{\text{Wing Profile Drag}}{\text{Total Aircraft Drag}}$
Transport	~ 1/3
Business jet	~ 1/3
Low-speed GA	> 1/3
UAV	1/3 to 1/2
Sailplane	> 1/2

To minimize wing profile drag, the figure of merit FOM applicable to aircraft having their wing area determined by a minimum-speed requirement (usually landing speed) should be maximized:

$$FOM = \frac{c_{l,\,max}}{c_{d,\,cruise}}$$

where $c_{l,max}$ is the section maximum lift coefficient and $c_{d,cruise}$ is the cruise section profile-drag coefficient. (See ref. 1.) [Note that the figure of merit is expressed in terms of section (airfoil) characteristics, not aircraft characteristics.] The figure of merit can be interpreted as follows. The wing area, and therefore the aircraft wetted area, can be reduced if a higher maximum lift coefficient is achieved, resulting in lower drag. The wing profile drag can also be reduced if a lower section profile-drag coefficient is achieved. This figure of merit applies to almost all classes of aircraft. For those aircraft having their wing area determined by a fuel-volume requirement (e.g., business jets), reducing the section profile-drag coefficient is even more beneficial.

Three approaches have become accepted for the reduction of wing profile drag. One approach is to employ a high-lift system (e.g., leading-edge slat plus double- or triple-slotted, Fowler flap) to achieve a higher maximum lift coefficient. (See, for example, ref. 2.) This approach has several disadvantages. Almost no laminar flow can be achieved because of the disturbances introduced by the slat, which results in a high section profile-drag coefficient. The maximum lift coefficient is limited to about 4, which limits the reduction in wing area. High-lift systems are complex, both mechanically and structurally, resulting in higher weight and cost. This approach can provide a maximum wing profile-drag reduction of about 50 percent compared to a conventional, turbulent-flow wing with no high-lift system and has been adopted for all current transport aircraft. Active high-lift systems (e.g., blown flaps and circulation control) have demonstrated very high lift coefficients but the cost, complexity, and potentially disastrous failure modes have prevented their adoption in production aircraft.

A second approach is to employ a natural-laminar-flow (NLF) airfoil to achieve a lower profile-drag coefficient. (See, for example, ref. 3.) By appropriate airfoil shaping, extensive ($\geq$ 30-percent chord) laminar flow can be achieved on both the upper and lower wing surfaces. The extent of laminar flow is limited to about 70-percent chord by the pressure-recovery gradient along the aft portion of the airfoil and by leading-edge sweep. The recovery gradient becomes steeper as the extent of the favorable gradient along the forward portion of the airfoil increases. The recovery gradient eventually reaches a limit beyond which trailing-edge separation occurs, resulting in a lower maximum lift coefficient and a correspondingly lower figure of merit. Leading-edge sweep restricts the extent of laminar flow because it introduces crossflow instabilities that lead to transition. This approach can also provide a wing profile-drag reduction of about 50 percent compared to a conventional, turbulent-flow wing and has been adopted for most current general-aviation aircraft, including business jets, as well as unmanned aerial vehicles and all sailplanes. It does, however, require more stringent construction techniques.

A third approach is to employ a laminar-flow-control (LFC) airfoil to achieve a lower profile-drag coefficient. (See, for example, ref. 4.) By incorporating suction through porous or slotted, wing skins, 100-percent-chord laminar flow can be achieved on both the upper and lower wing surfaces. LFC systems are very complex, mechanically, structurally, and operationally, resulting in higher weight and cost. This approach can provide a wing profile-drag reduction of about 75 percent compared to a conventional, turbulent-flow wing but has yet to be adopted for any production aircraft.

For the present effort, a new approach, called a slotted, natural-laminar-flow (SNLF) airfoil, is employed. The SNLF airfoil concept is similar in nature to the slotted, supercritical airfoil concept (ref. 5).

SYMBOLS

C_p	pressure coefficient
c	airfoil chord, m
c_d	section profile-drag coefficient
c_l	section lift coefficient
c_m	section pitching-moment coefficient about quarter-chord point
M	Mach number
R	Reynolds number based on free-stream conditions and airfoil chord
t	airfoil thickness, m
x	airfoil abscissa, m
α	angle of attack relative to x-axis, deg

Subscripts:

dd	drag divergence
ll	lower limit of low-drag range
ls	lower surface
max	maximum
T	transition
ul	upper limit of low-drag range
us	upper surface
0	zero lift

Abbreviations:

LFC	laminar flow control
NASA	National Aeronautics and Space Administration

NLF natural laminar flow

SNLF slotted, natural laminar flow

AIRFOIL DESIGN

OBJECTIVES AND CONSTRAINTS

The design specifications for the airfoil are contained in table I. The specifications were distilled from the physical and performance characteristics of seven light business-jet designs. The following aircraft were used: Adam Aircraft A700, Aerostar FJ-100, Beechcraft Premier I, Cessna Citation Bravo and CJ1, Honda R&D HondaJet, and VisionAire Vantage. The specifications encompass the requirements of almost all the aircraft well.

Two primary objectives are evident. The first objective is to achieve a maximum lift coefficient of at least 1.55 at a Mach number of 0.10 and a Reynolds number of 3×10^6, which corresponds to the tip chord at minimum speed. A requirement related to this objective is that the maximum lift coefficient not decrease significantly with transition fixed near the leading edge on both surfaces. In addition, the airfoil should exhibit docile stall characteristics. The second objective is to obtain low profile-drag coefficients over the range of lift coefficients from 0.20 at a Mach number of 0.65 and a Reynolds number of 12×10^6, which corresponds to the root chord at the cruise condition, to 0.40 at a Mach number of 0.30 and a Reynolds number of 12×10^6, which corresponds to the root chord at the climb condition. (The second specification regarding the upper limit of the low-drag, lift-coefficient range, which corresponds to the high-altitude, cruise condition, is not critical for the airfoil design.)

It should be noted that, while the cruise Mach number is lower than those of larger business-jet and transport aircraft, higher cruise speeds do not yield significant time savings because the typical range of light, business jets is only about 2000 km (1000 nm); the negative impact of higher speeds on fuel efficiency outweighs the small gain in block time. The drag-divergence Mach number at a lift coefficient of 0.25 for a Reynolds number of 12×10^6, which corresponds to the root chord at the high-altitude, maximum-speed condition, should be greater than 0.70.

One major constraint was placed on the design of the airfoil. The airfoil thickness should equal 15-percent chord. No constraint was placed on the pitching-moment coefficient.

PHILOSOPHY

Given the above objectives and constraint, certain characteristics of the design are apparent. The following sketch illustrates a drag polar that meets the goals for this design.

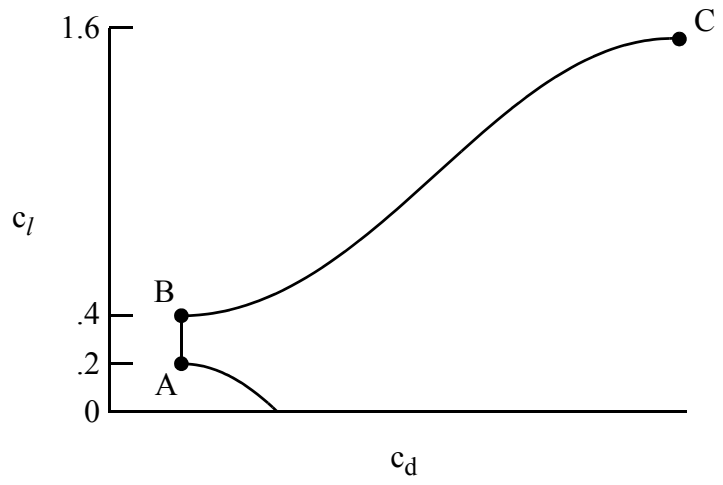

Sketch 1

Point A is the lower limit of the low-drag, lift-coefficient range; point B, the upper limit. The profile-drag coefficient increases very rapidly outside the low-drag range because boundary-layer transition moves quickly toward the leading edge with increasing (or decreasing) lift coefficient. This feature results in a leading edge that produces a suction peak at higher lift coefficients, which ensures that transition on the upper surface will occur very near the leading edge. Thus, the maximum lift coefficient, point C, occurs with turbulent flow along the entire upper surface and, therefore, should be relatively insensitive to roughness at the leading edge.

A two-element airfoil concept is used to meet the design requirements. The pressure distribution at point A is illustrated in sketch 2. (The sonic pressure coefficient at this Mach number is −1.01, denoted by the horizontal, dotted line in sketch 2.)

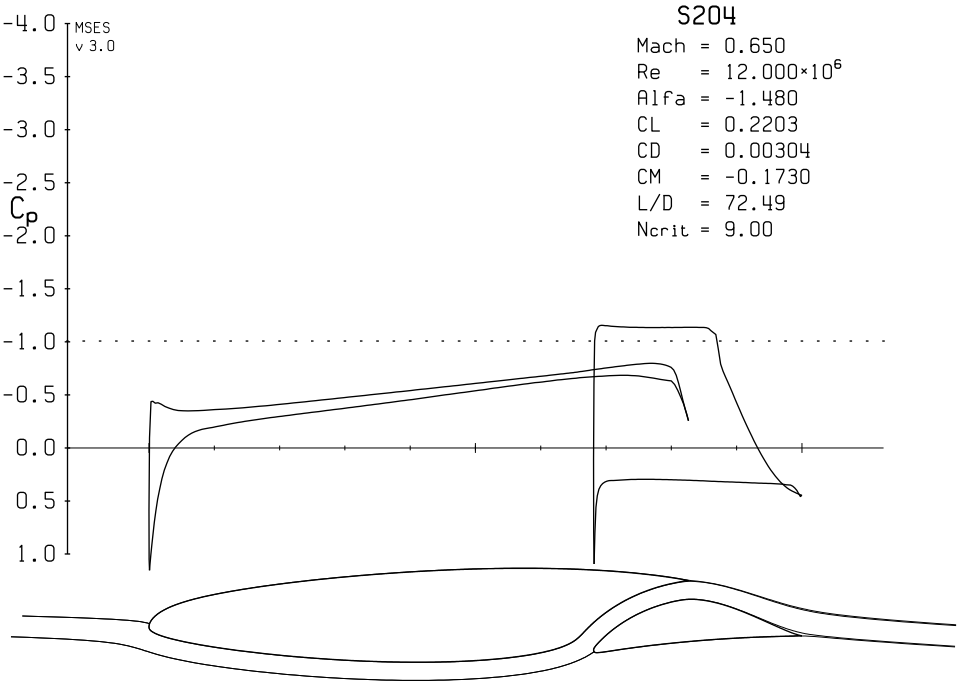

Sketch 2

Because the aft element eliminates the requirement that the pressure at the trailing edge of the fore element recover to free stream (see ref. 6), the favorable pressure gradient can extend further aft. For the slotted, natural-laminar-flow (SNLF) airfoil concept, the favorable gradient extends along both surfaces of the fore element to near its trailing edge. Thus, the fore element is almost entirely laminar. The aft element then provides the necessary recovery to free-stream pressure. Because the wake of the fore element does not impinge on the aft element, the aft element can also achieve significant extents of laminar flow.

The SNLF airfoil concept allows the extent of natural laminar flow to be increased beyond the limit previously discussed. Thus, the concept allows lower section profile-drag coefficients to be achieved without having to resort to the complexity and cost of LFC. The concept also allows high maximum lift coefficients to be achieved without variable geometry. The SNLF airfoil shape is not radically different from conventional airfoil shapes—no more than conventional, NLF airfoils are from conventional, turbulent-flow airfoils. Unlike conventional airfoils with slotted flaps, however, the SNLF airfoil has no nested configuration; the slot between the fore and aft elements is always open.

EXECUTION

The Eppler Airfoil Design and Analysis Code (refs. 7 and 8), a subcritical, single-element code, was used to design the initial fore- and aft-element shapes. The MSES code (ref. 9), a transonic, multielement code, was used to refine the shapes in the two-element configuration.

The airfoil is designated the S204. The airfoil shape is shown in figure 1. The airfoil thickness is 14-percent chord, which is less than the design constraint of $t/c = 0.15$, primarily to meet the cruise Mach-number objective.

THEORETICAL PROCEDURE

The pressure distributions and section characteristics are predicted using the method of reference 9 at a Mach number of 0.10 for Reynolds numbers of 2×10^6, 3×10^6, 4×10^6, and 6×10^6 and at Mach numbers of 0.30, 0.50, 0.60, and 0.65 for Reynolds numbers of 4×10^6, 6×10^6, 9×10^6, and 12×10^6. The computations were performed with transition free using a critical amplification factor of 9, although, because of laminar separation bubbles predicted near the trailing edge of the fore element, transition was fixed on both the upper and lower surfaces of the fore element at 97 percent of the fore-element chord (i.e., $x/c = 0.80$). Note that the method of reference 9 does not model the effect of Görtler instabilities (ref. 10) on the laminar boundary layer. A cursory evaluation of this effect indicates that these instabilities may lead to transition in the concave region of the lower surface of the fore element.

Computations were also performed with transition fixed at 2-percent chord on the upper surface and 5-percent chord on the lower surface of both elements for all Mach numbers except 0.10 for which transition was fixed at the same locations on the aft element and on the upper surface of the fore element but at 10-percent chord on the lower surface of the fore element to account for the more aft location of the stagnation point at high lift coefficients. Note that all the fixed-transition locations are specified relative to the chord of the respective element.

Because the right sides of the figures showing the transition locations and section characteristics contain several curves, an explanatory example with transition free is given in sketch 3, where the various curves are plotted with different line types. Note that the transition locations on the aft element are downstream of those on the fore element.

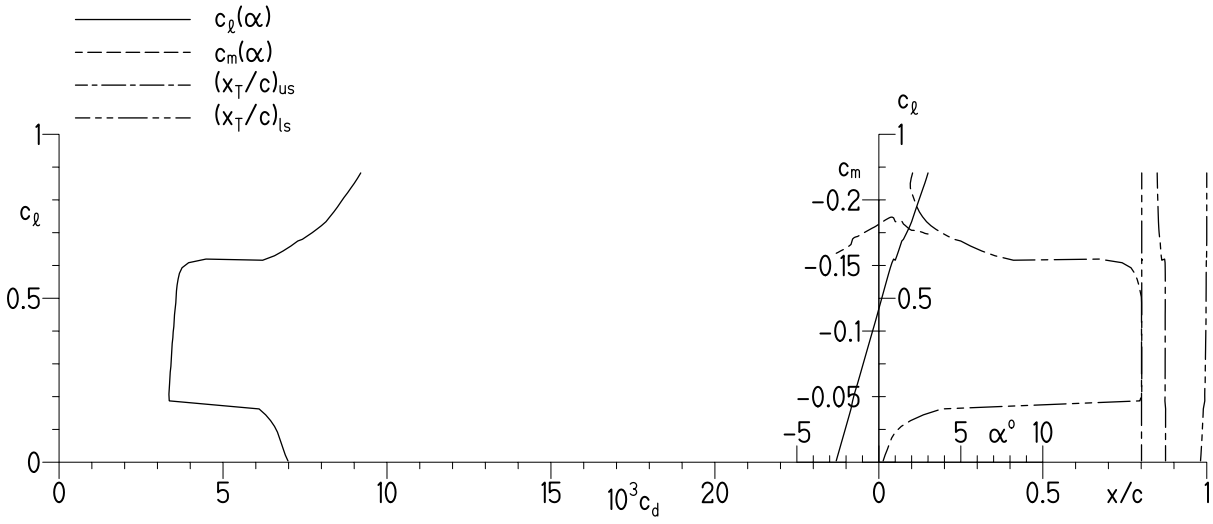

Sketch 3

DISCUSSION OF RESULTS

PRESSURE DISTRIBUTIONS

The pressure distributions at various angles of attack with transition free at a Mach number of 0.10 and a Reynolds number of 3×10^6 are shown in figure 2 and at Mach numbers of 0.30, 0.50, 0.60, and 0.65 and a Reynolds number of 12×10^6, in figures 3, 4, 5, and 6, respectively.

TRANSITION LOCATION

The variations of boundary-layer transition location on the fore and aft elements with lift coefficient are shown in figures 7 through 11. In general, within the low-drag, lift-coefficient range, laminar flow extends essentially to the trailing edge on both surfaces of the fore element, to about 60-percent of the aft-element chord on the upper surface of the aft element, and to the trailing edge on the lower surface of the aft element.

SECTION CHARACTERISTICS

Mach Number and Reynolds Number Effects

The section characteristics at a Mach number of 0.10 and Reynolds numbers of 2×10^6, 3×10^6, 4×10^6, and 6×10^6 with transition free are shown in figure 7. For a Reynolds number of 3×10^6 (fig. 7(b)), the maximum lift coefficient is predicted to be 2.13, which meets the design objective of $c_{l,\max} \geq 1.55$.

The section characteristics at a Mach number of 0.30 and Reynolds numbers of 4×10^6, 6×10^6, 9×10^6, and 12×10^6 with transition free are shown in figure 8. For a Reynolds number of 12×10^6 (fig. 8(d)), a low profile-drag coefficient is predicted at a lift coefficient of about 0.2, but no low-drag range of lift coefficients is predicted. Thus, the design objective of $c_{l,\text{ul}} = 0.40$ has not been met. The zero-lift pitching-moment coefficient is predicted to be –0.133.

The section characteristics at Mach numbers of 0.50 and 0.60 and Reynolds numbers of 4×10^6, 6×10^6, 9×10^6, and 12×10^6 with transition free are shown in figures 9 and 10, respectively.

The section characteristics at a Mach number of 0.65 and Reynolds numbers of 4×10^6, 6×10^6, 9×10^6, and 12×10^6 with transition free are shown in figure 11. For a Reynolds number of 12×10^6 (fig. 11(d)), low drag coefficients are predicted over the range of lift coefficients from 0.22 to 0.52. Thus, the lower limit of the low-drag range is higher than the design objective of $c_{l,\text{ll}} = 0.20$. For a Reynolds number of 9×10^6 (fig. 11(c)), low drag coefficients are predicted over the range of lift coefficients from 0.19 to 0.59. Thus, the upper limit of the low-drag range is higher than the design objective of $c_{l,\text{ul}} = 0.40$. Within the low-drag range, no wave drag is predicted. The zero-lift pitching-moment coefficient is predicted to be –0.162.

The effect of Mach number on the section characteristics with transition free is summarized in figure 12. In general, the zero-lift angle of attack is relatively unaffected by Mach number. The lift-curve slope, the minimum drag coefficient, the width of the low-drag range, and the magnitude of the pitching-moment coefficient increase with increasing Mach number. Based on computations performed using the method of reference 9, the drag-divergence Mach number with transition free is predicted to be greater than 0.70, which meets the design objective.

The effect of Reynolds number on the section characteristics with transition free is summarized in figure 13. In general, the zero-lift angle of attack, the lift-curve slope, and the pitching-moment coefficient are relatively unaffected by Reynolds number. The maximum lift coefficient (fig. 13(a)) increases with increasing Reynolds number. The minimum drag coefficient and the width of the low-drag range decrease with increasing Reynolds number.

Effect of Roughness

The effect of roughness on the section characteristics is shown in figures 7 through 11. The maximum lift coefficient at a Mach number of 0.10 and a Reynolds number of 3×10^6 with transition fixed (fig. 7(b)) is predicted to be 2.10, a decrease of approximately 1 percent from that with transition free. Thus, the design requirement has been satisfied. In general, the magnitudes of the zero-lift angle of attack and the pitching-moment coefficient decrease with transition fixed primarily because the roughness on the aft element induces trailing-edge separation on the upper surface of that element. The lift-curve slope is relatively unaffected by the roughness, but the drag coefficients are, of course, adversely affected. The drag increase is larger than that for a single-element airfoil of the same thickness, however, because of the greater wetted surface length of the two-element configuration and also because of the separation on the aft-element upper surface.

The effect of Mach number on the section characteristics with transition fixed is summarized in figure 14. In general, the magnitude of the zero-lift angle of attack decreases with increasing Mach number. The lift-curve slope and the minimum drag coefficient increase with increasing Mach number. The magnitude of the pitching-moment coefficient is relatively unaffected by Mach number. The drag-divergence Mach number with transition fixed is predicted to be greater than 0.70, which meets the design objective.

The effect of Reynolds number on the section characteristics with transition fixed is summarized in figure 15. In general, the magnitudes of the zero-lift angle of attack, the maximum lift coefficient, and the pitching-moment coefficient increase with increasing Reynolds number. The lift-curve slope is relatively unaffected by Reynolds number. The minimum drag coefficient decreases with increasing Reynolds number.

CONCLUDING REMARKS

A 14-percent-thick, slotted, natural-laminar-flow airfoil, the S204, for light business-jet applications has been designed and analyzed theoretically. The two primary objectives of a high maximum lift coefficient, relatively insensitive to leading-edge roughness, and low profile-drag coefficients have been achieved. The drag-divergence Mach number is predicted to be greater than 0.70.

REFERENCES

1. Maughmer, Mark D.; and Somers, Dan M.: Figures of Merit for Airfoil/Aircraft Design Integration. AIAA Paper 88-4416, Sept. 1988.

2. Smith, A. M. O.: High-Lift Aerodynamics. AIAA Paper 74-939, Aug. 1974.

3. Jacobs, Eastman N.: Preliminary Report on Laminar-Flow Airfoils and New Methods Adopted for Airfoil and Boundary-Layer Investigations. NACA WR L-345, 1939 (formerly, NACA ACR).

4. Pfenninger, Werner: Investigations on Reductions of Friction on Wings, in Particular by Means of Boundary Layer Suction. NACA TM 1181, 1947. (Translated from Mitteilungen aus dem Institut für Aerodynamik an der Eidgenössischen Technischen Hochschule Zürich, Nr. 13, 1946.)

5. Whitcomb, Richard T.; and Clark, Larry R.: An Airfoil Shape for Efficient Flight at Supercritical Mach Numbers. NASA TM X-1109, 1965.

6. Maughmer, Mark D.: Trailing Edge Flow Conditions as a Factor in Airfoil Design. Ph.D. Dissertation, Univ. of Illinois, 1983.

7. Eppler, Richard: Airfoil Design and Data. Springer-Verlag (Berlin), 1990.

8. Eppler, Richard: Airfoil Program System "PROFIL00." User's Guide. Richard Eppler, c.2001.

9. Drela, M.: Design and Optimization Method for Multi-Element Airfoils. AIAA Paper 93-0969, Feb. 1993.

10. Görtler, H.: On the Three-Dimensional Instability of Laminar Boundary Layers on Concave Walls. NACA TM 1375, 1954.

TABLE I.- AIRFOIL DESIGN SPECIFICATIONS

Parameter	Value	Mach Number M	Reynolds Number R
Maximum lift coefficient $c_{l,max}$	≥ 1.55	0.10	3×10^6
Lower limit of low-drag, lift-coefficient range $c_{l,ll}$	0.20	0.65	12×10^6
Upper limit of low-drag, lift-coefficient range $c_{l,ul}$	0.40	0.65 0.30	9×10^6 12×10^6
Zero-lift pitching-moment coefficient $c_{m,0}$	—		
Drag-divergence Mach number M_{dd} at $c_l = 0.25$	≥ 0.70	—	12×10^6
Thickness t/c	0.15		

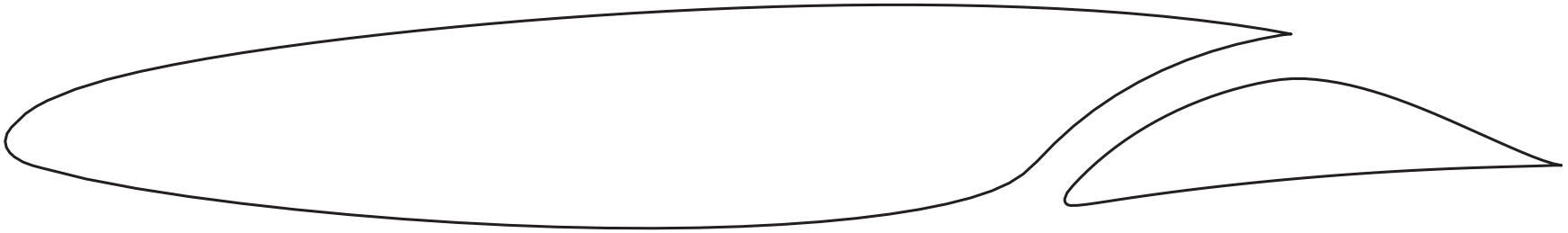

Figure 1.- S204 airfoil shape.

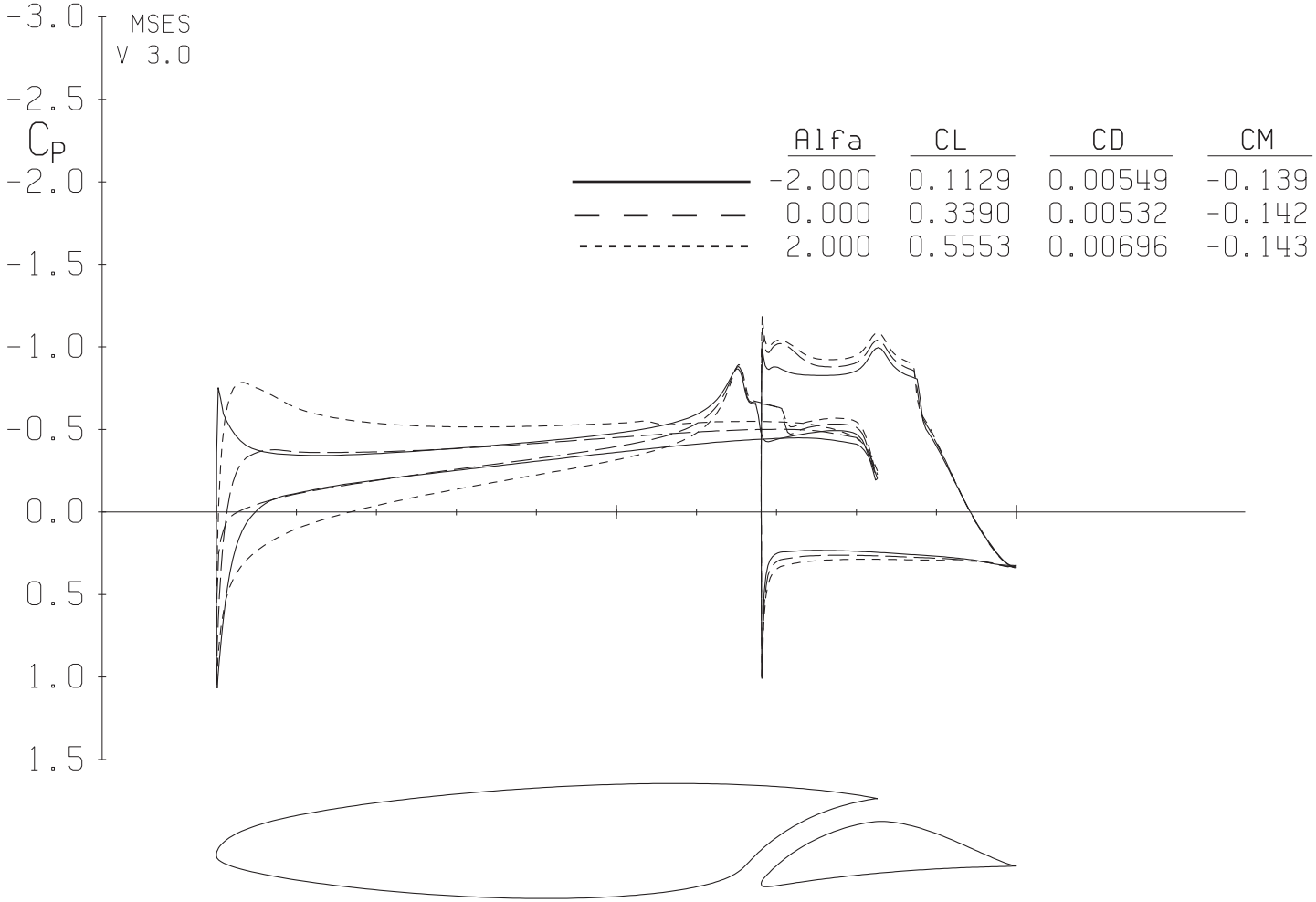

(a) $\alpha = -2°$, 0°, and 2°.

Figure 2.- Pressure distributions at M = 0.10 and R = 3×10^6 with transition free.

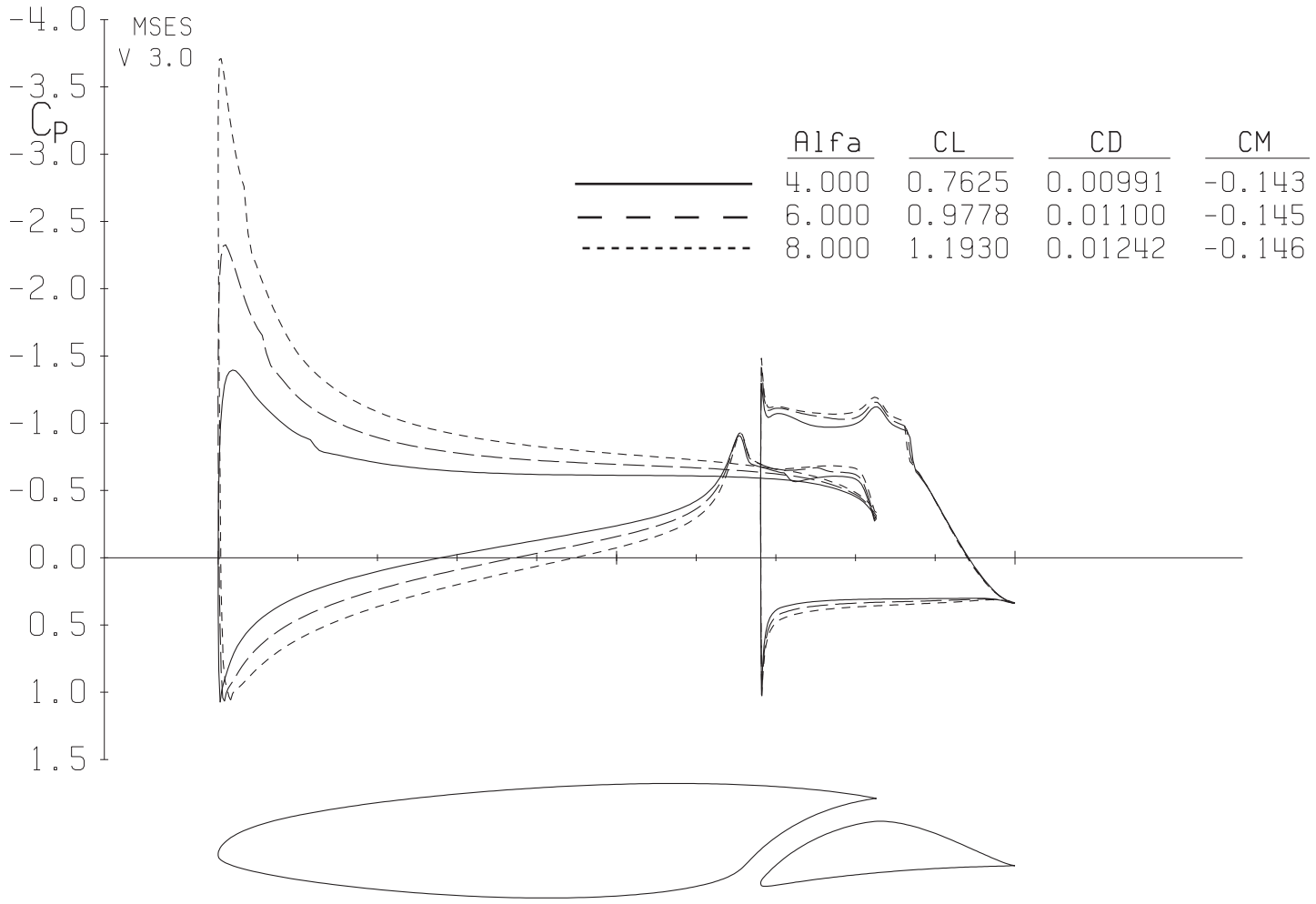

(b) $\alpha = 4°$, 6°, and 8°.

Figure 2.- Continued.

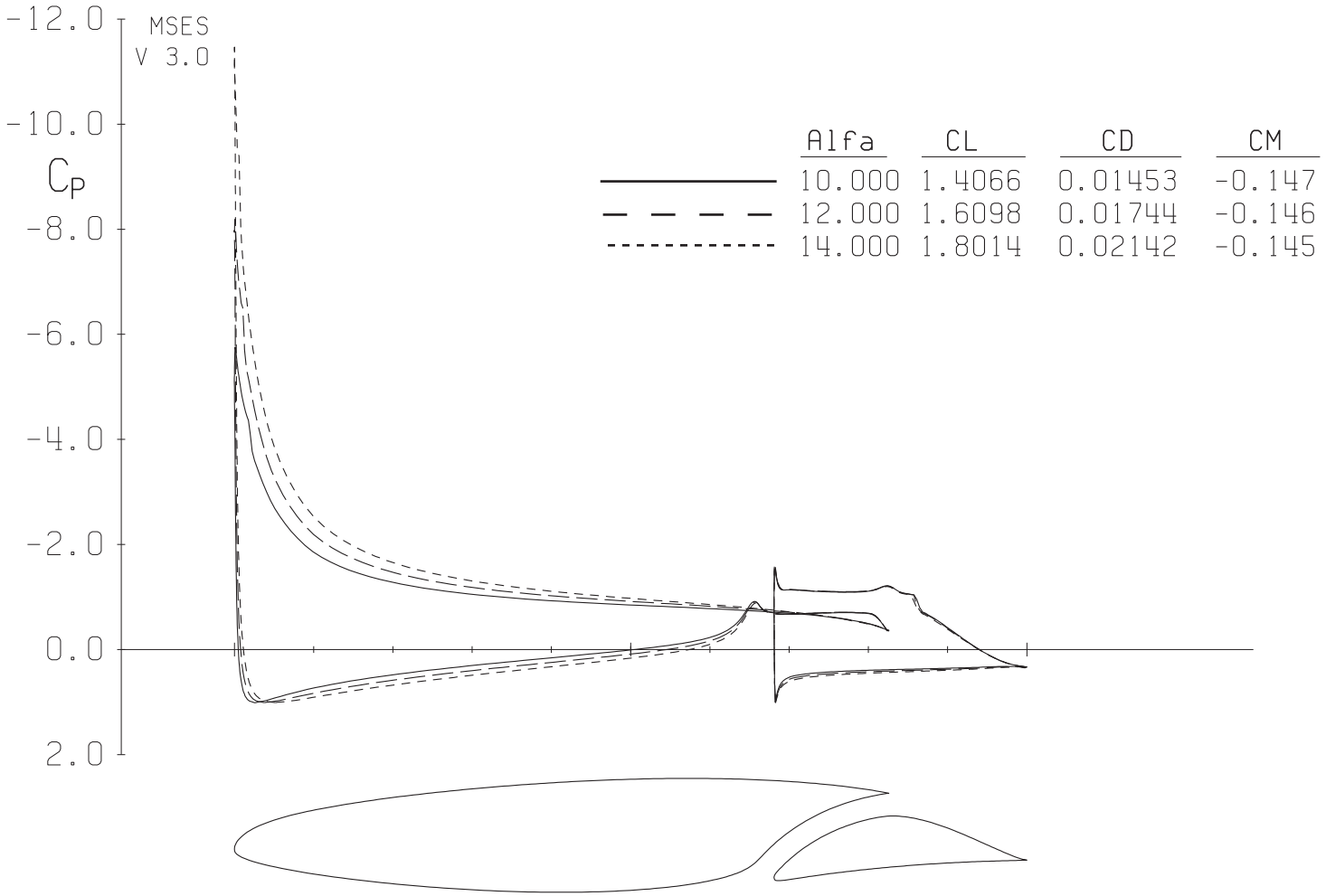

(c) $\alpha = 10°$, 12°, and 14°.

Figure 2.- Continued.

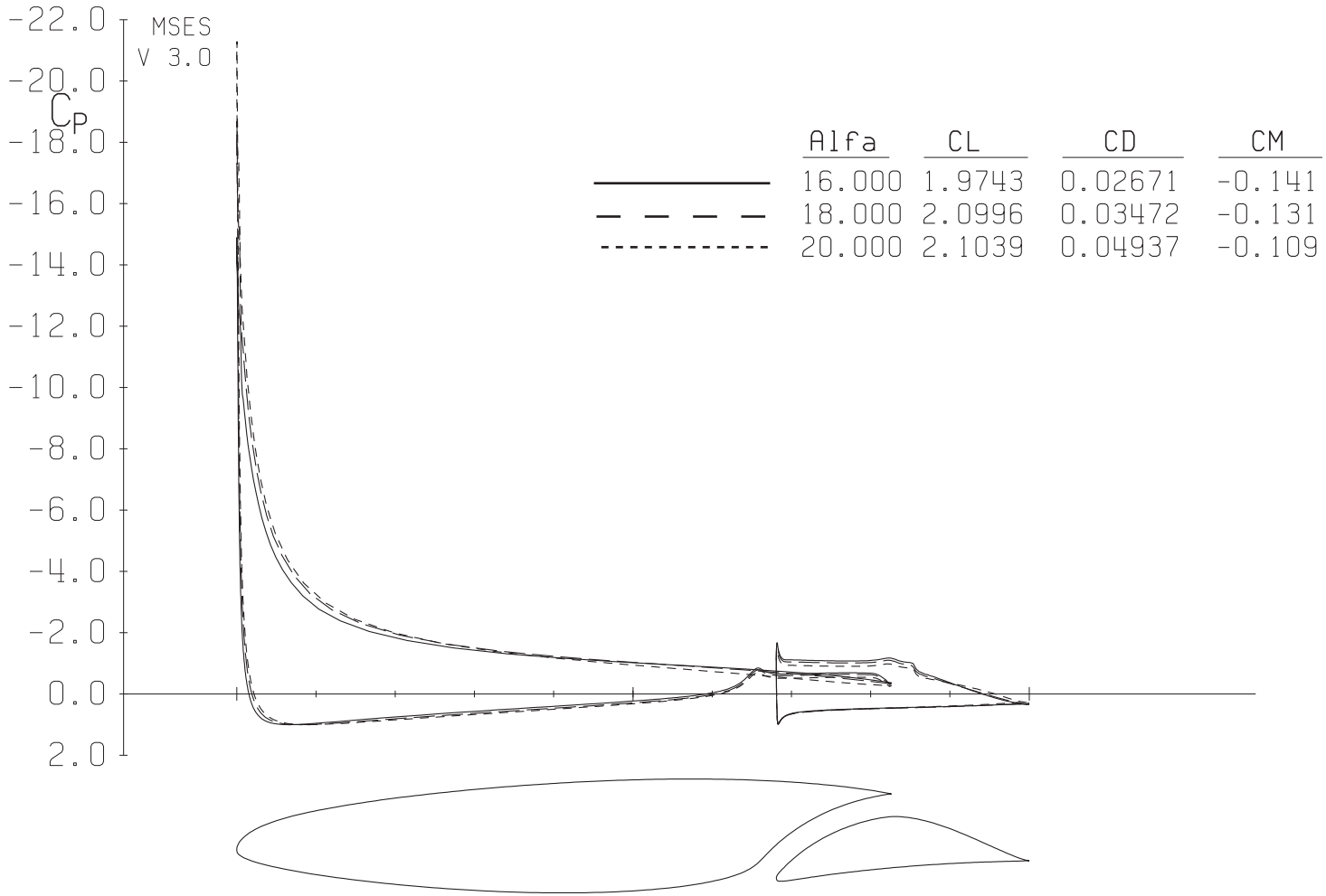

(d) $\alpha = 16°$, 18°, and 20°.

Figure 2.- Concluded.

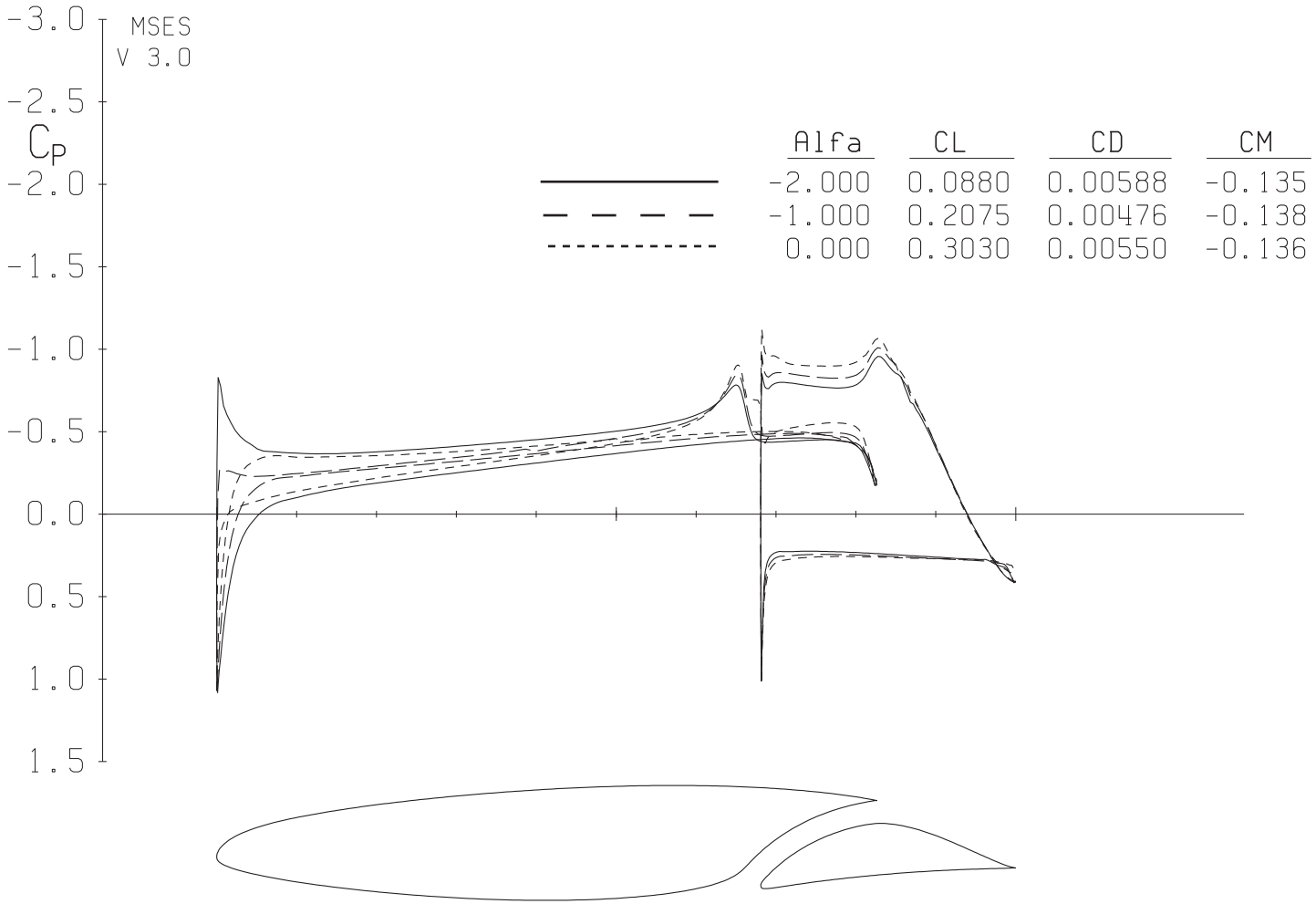

(a) $\alpha = -2°, -1°$, and $0°$.

Figure 3.- Pressure distributions at $M = 0.30$ and $R = 12 \times 10^6$ with transition free.

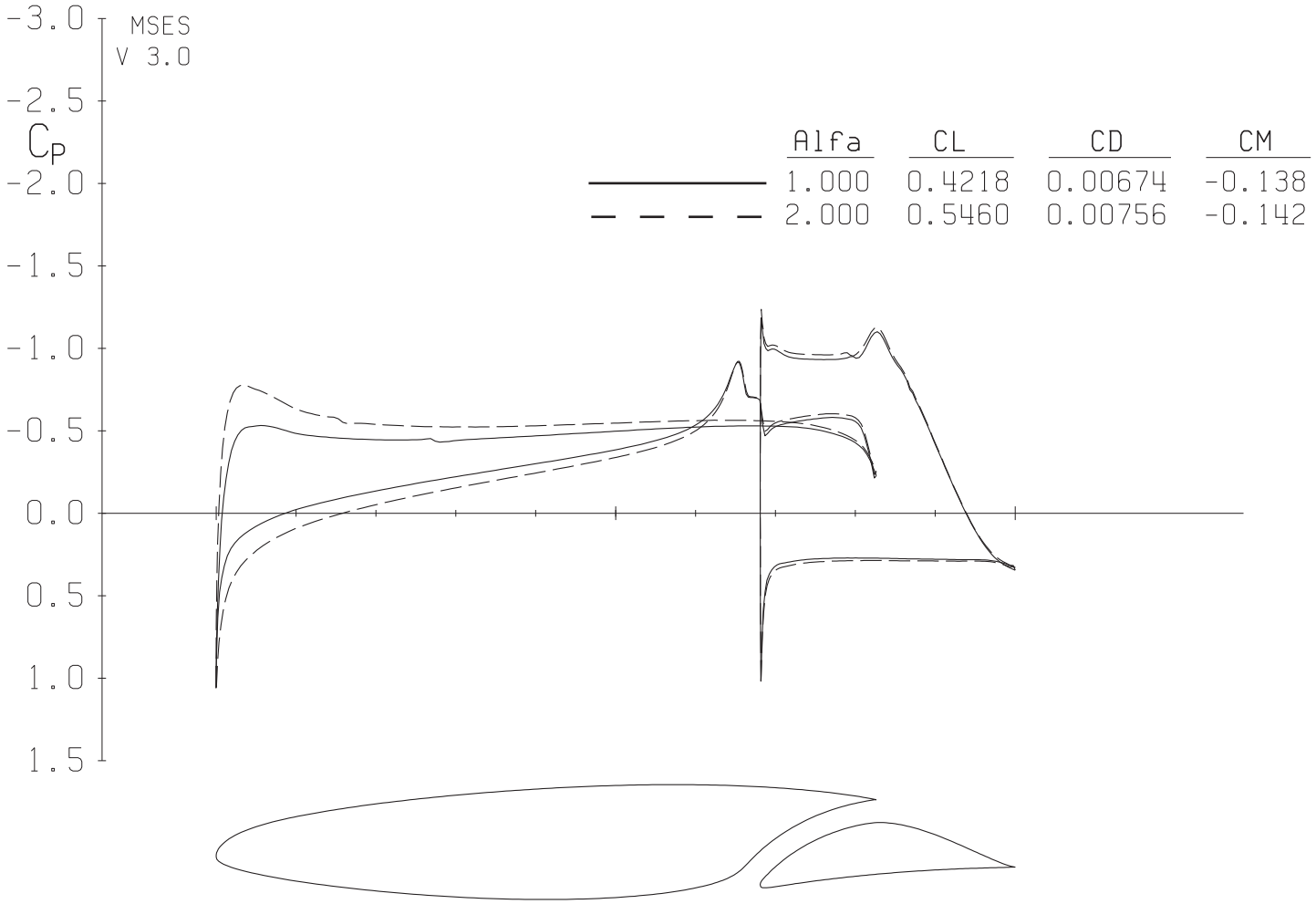

(b) $\alpha = 1°$ and $2°$.

Figure 3.- Concluded.

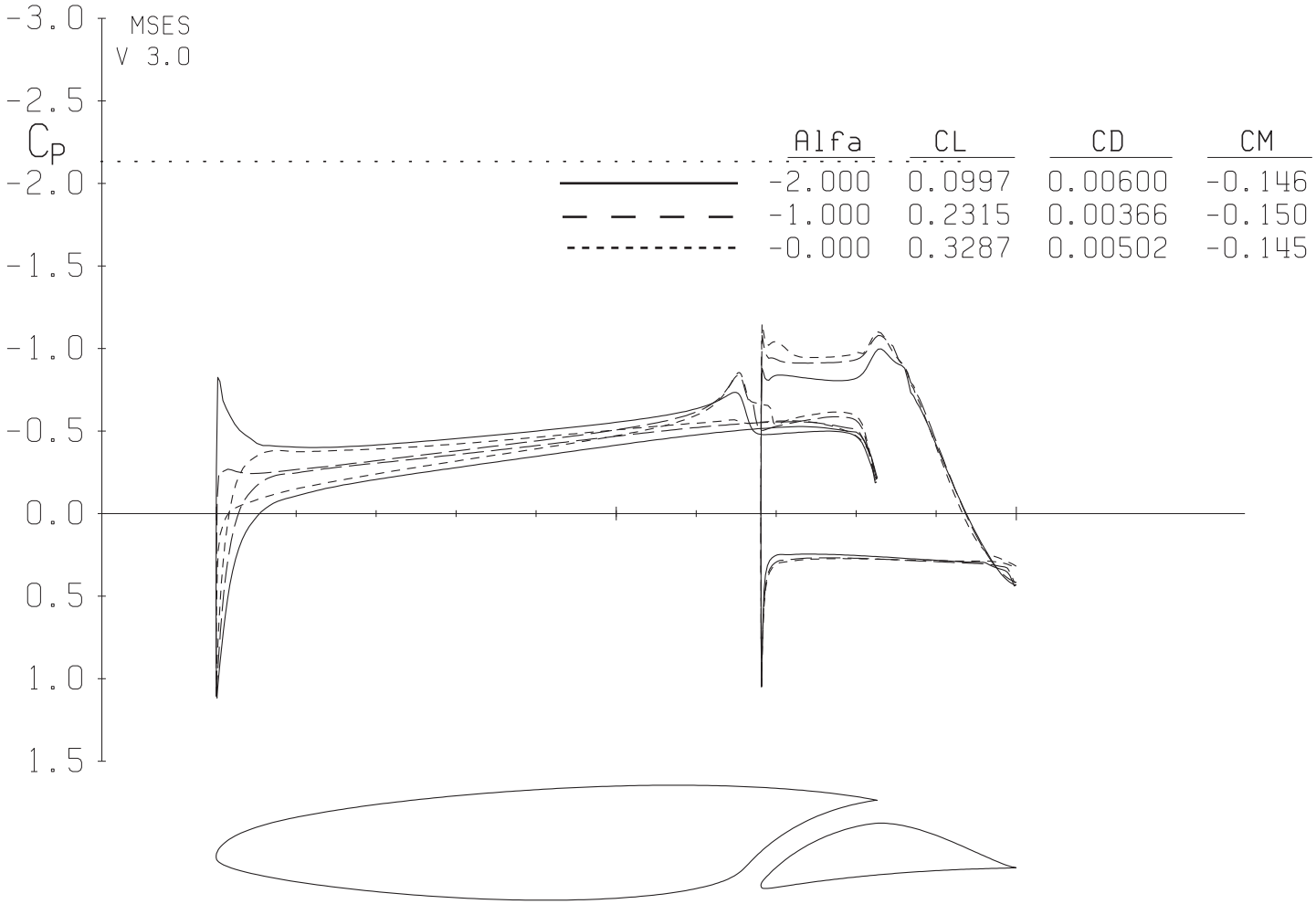

(a) $\alpha = -2°, -1°$, and $0°$.

Figure 4.- Pressure distributions at $M = 0.50$ and $R = 12 \times 10^6$ with transition free.

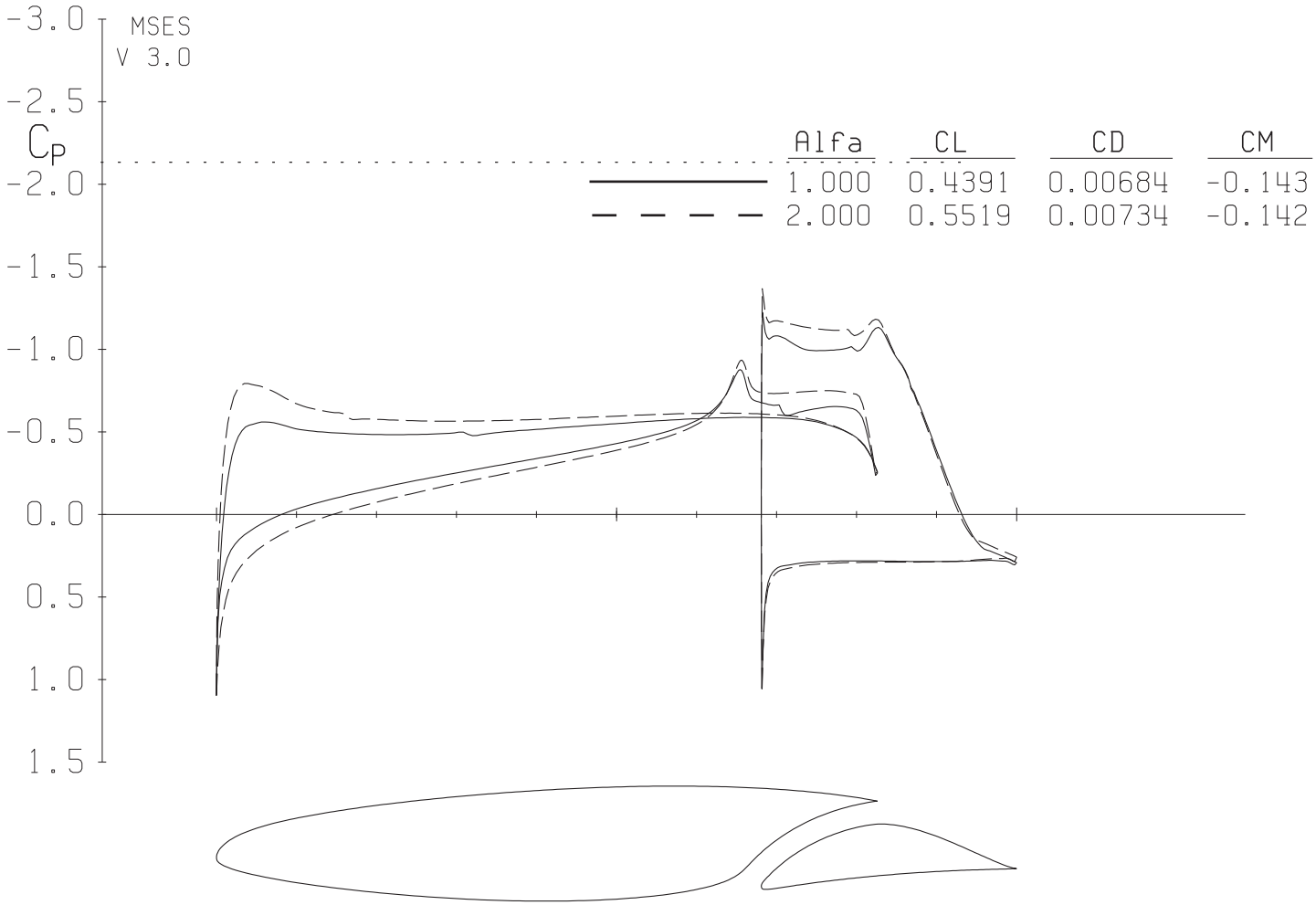

(b) $\alpha = 1°$ and $2°$.

Figure 4.- Concluded.

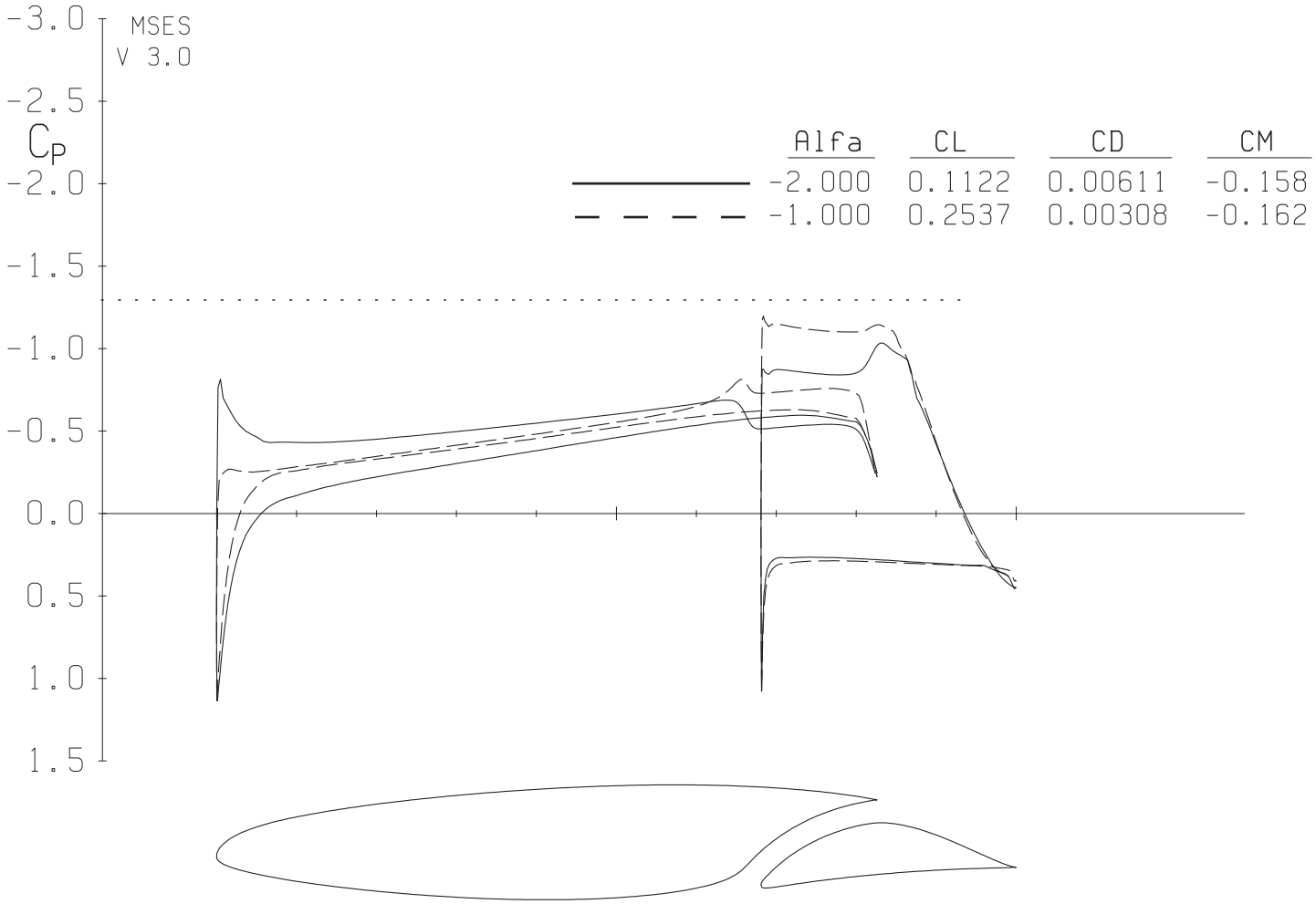

(a) $\alpha = -2°$ and $-1°$.

Figure 5.- Pressure distributions at $M = 0.60$ and $R = 12 \times 10^6$ with transition free.

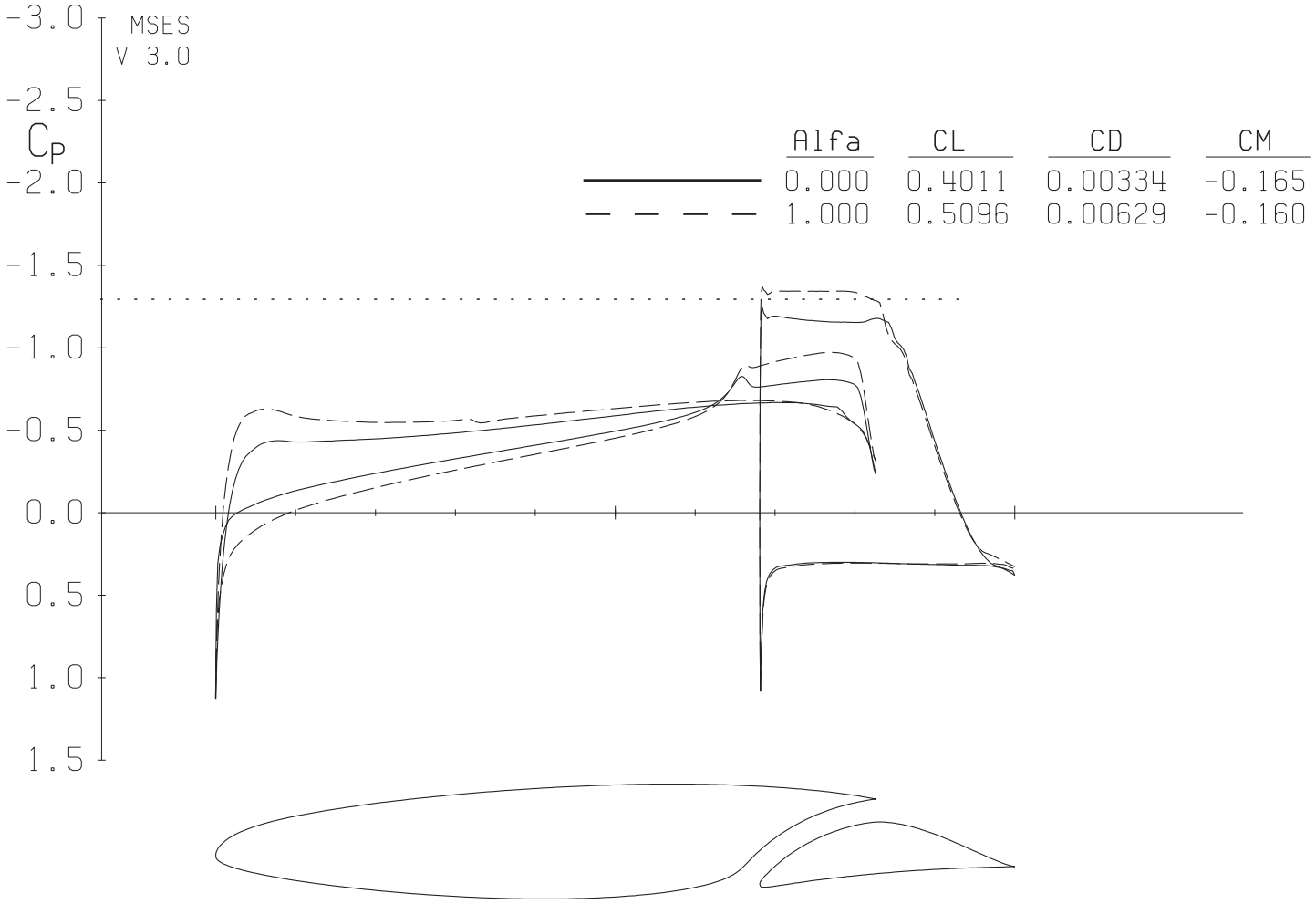

(b) $\alpha = 0°$ and 1°.

Figure 5.- Concluded.

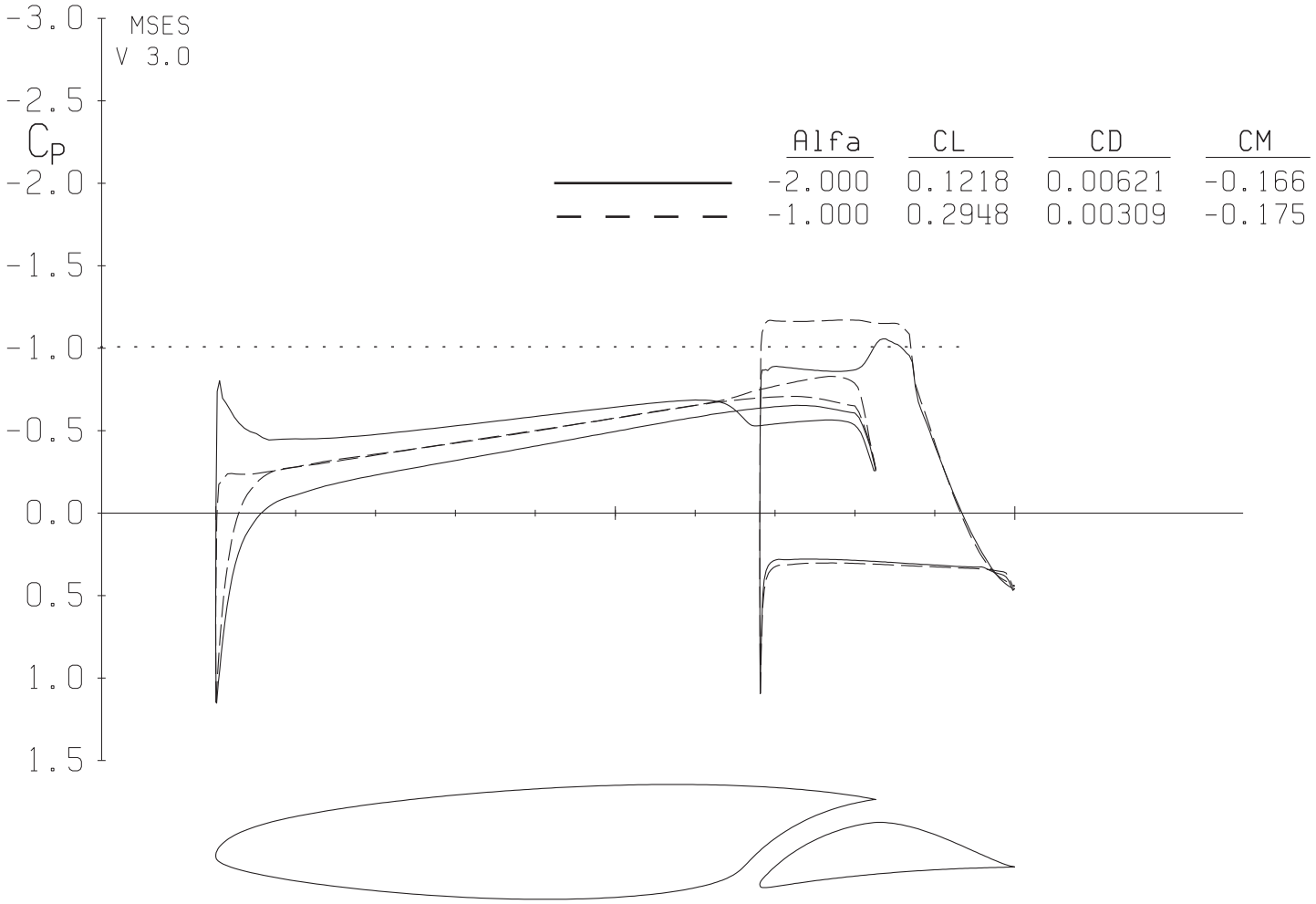

(a) $\alpha = -2°$ and $-1°$.

Figure 6.- Pressure distributions at $M = 0.65$ and $R = 12 \times 10^6$ with transition free.

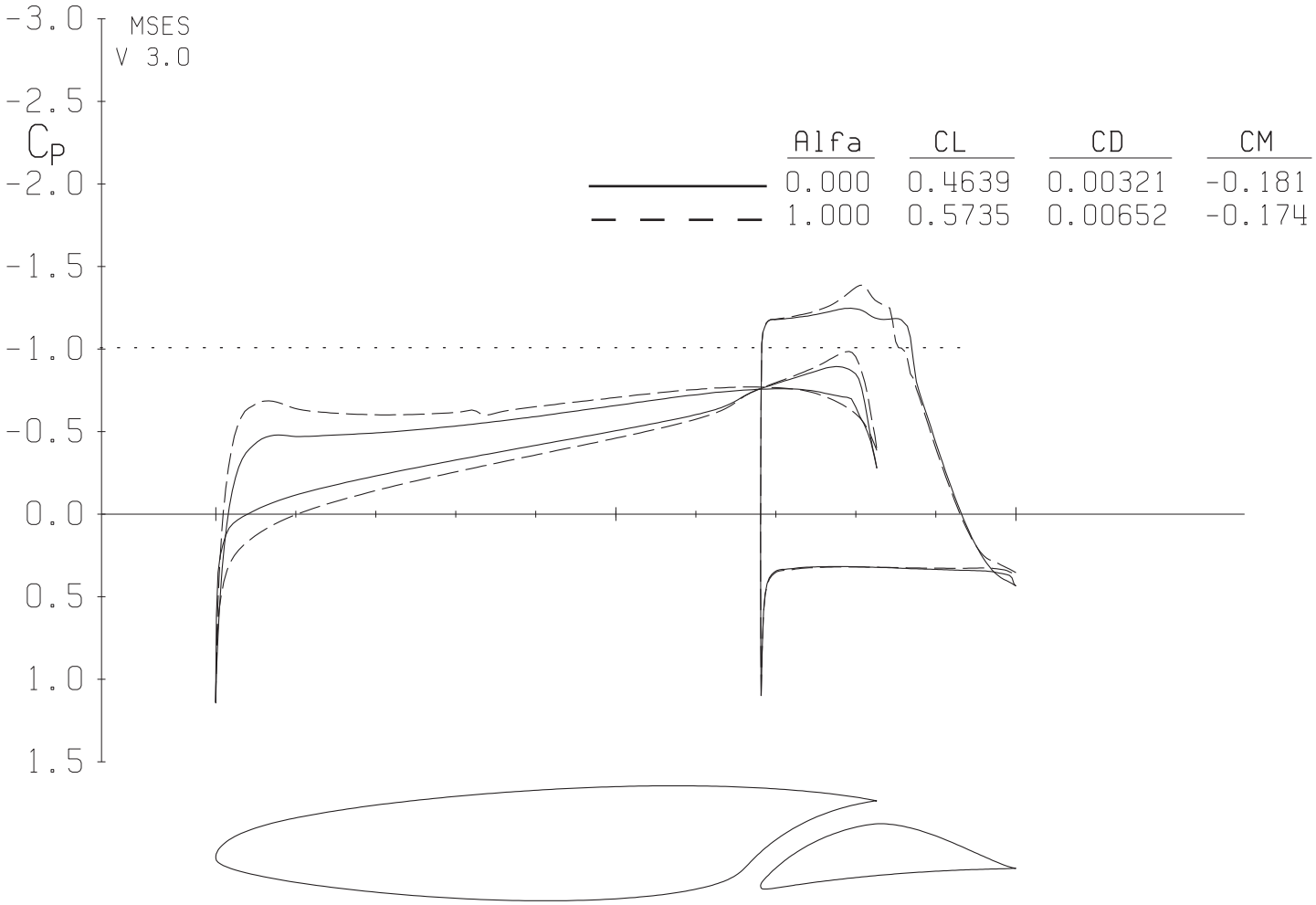

(b) $\alpha = 0°$ and 1°.

Figure 6.- Concluded.

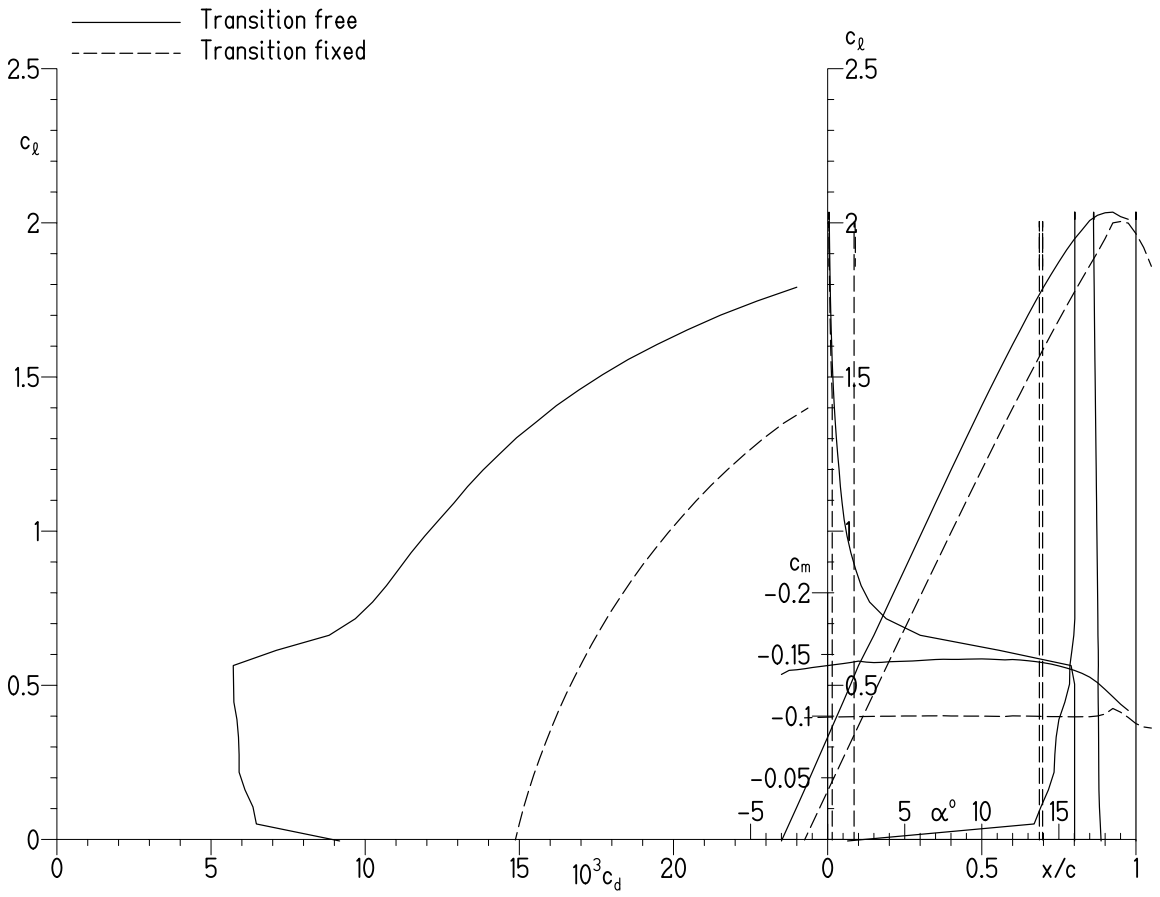

(a) $R = 2 \times 10^6$.

Figure 7.- Section characteristics at $M = 0.10$.

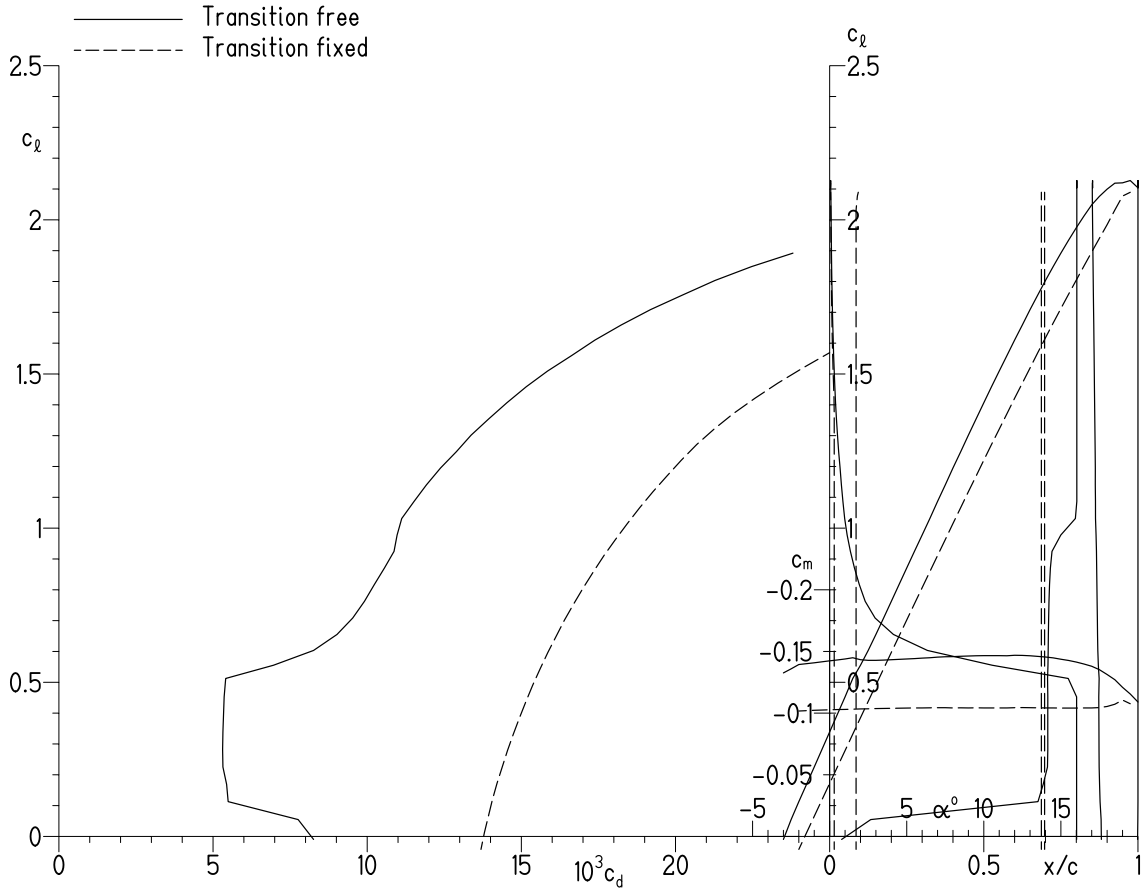

(b) $R = 3 \times 10^6$.

Figure 7.- Continued.

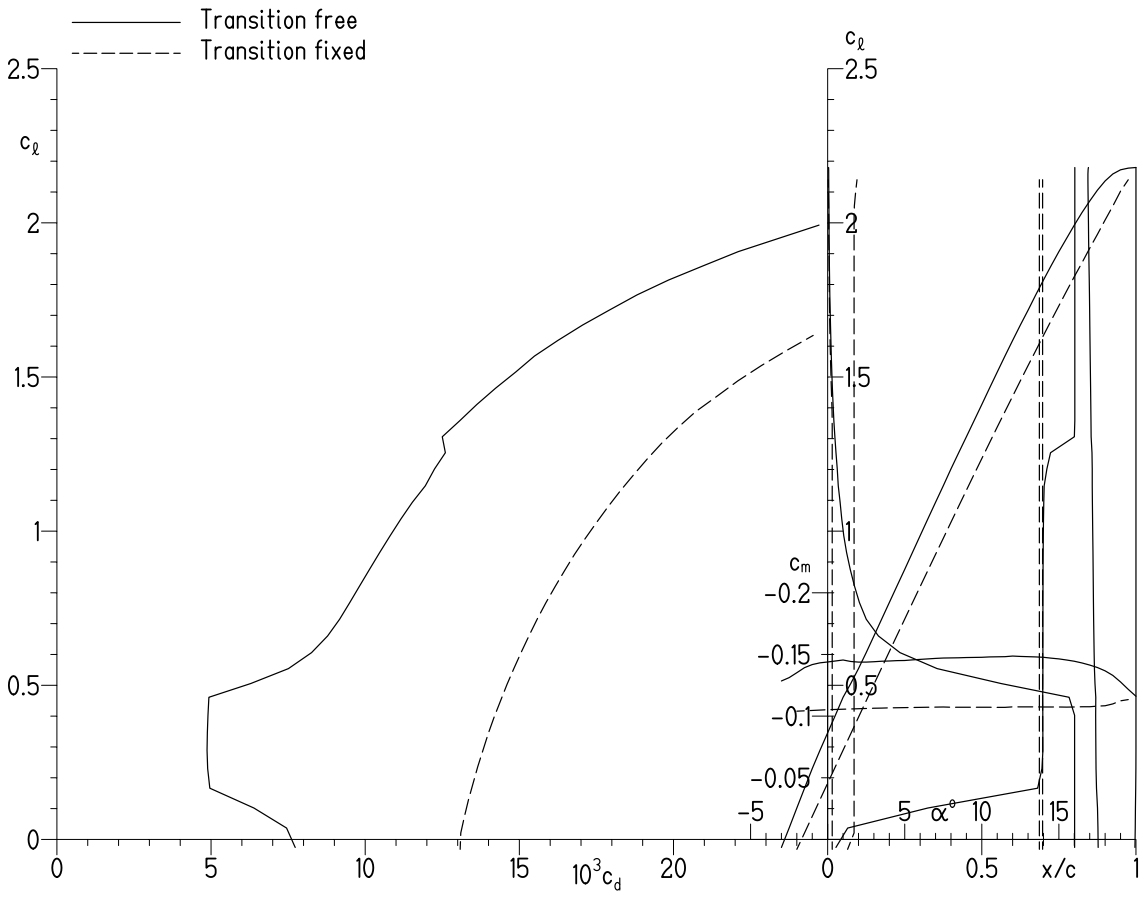

(c) $R = 4 \times 10^6$.

Figure 7.- Continued.

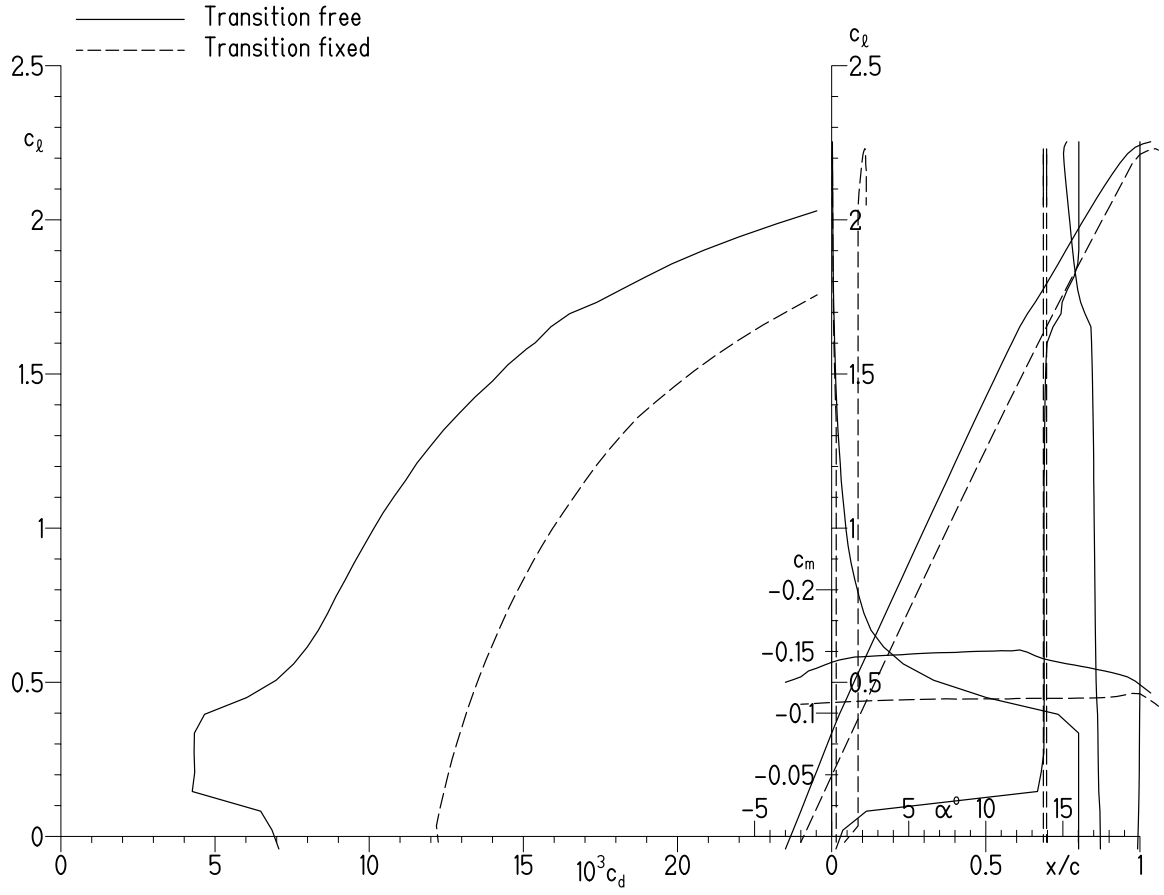

(d) $R = 6 \times 10^6$.

Figure 7.- Concluded.

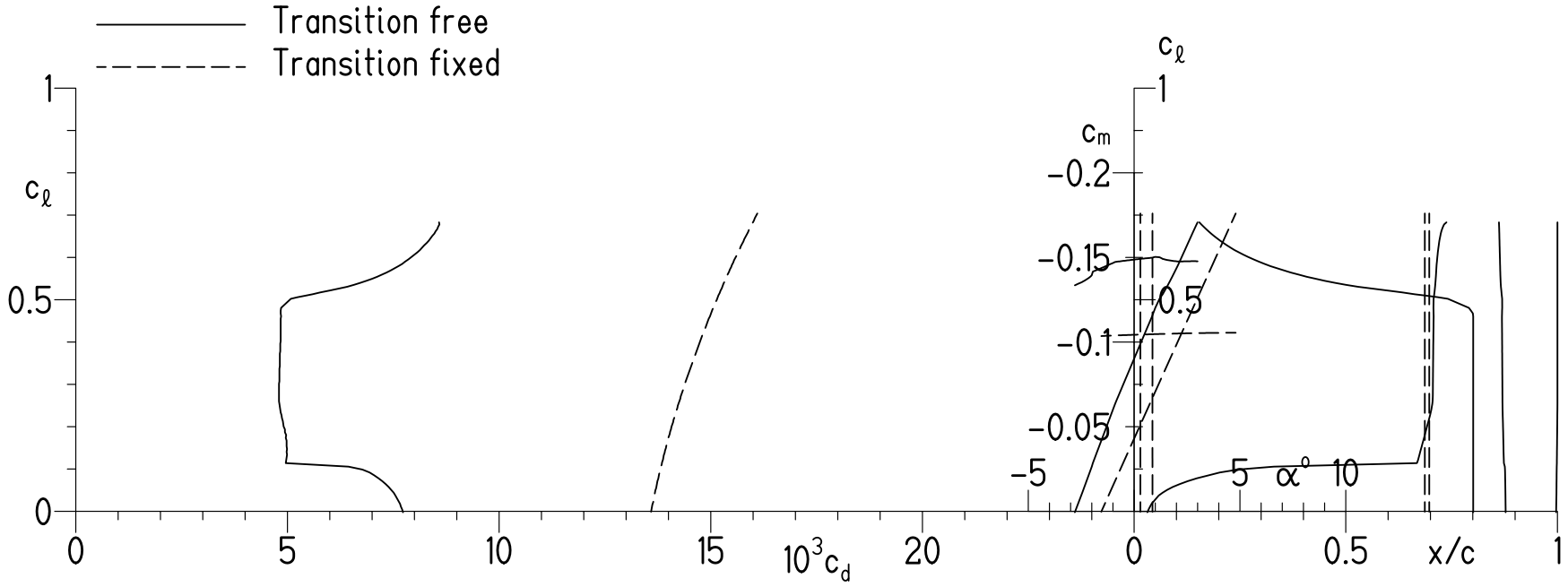

(a) $R = 4 \times 10^6$.

Figure 8.- Section characteristics at M = 0.30.

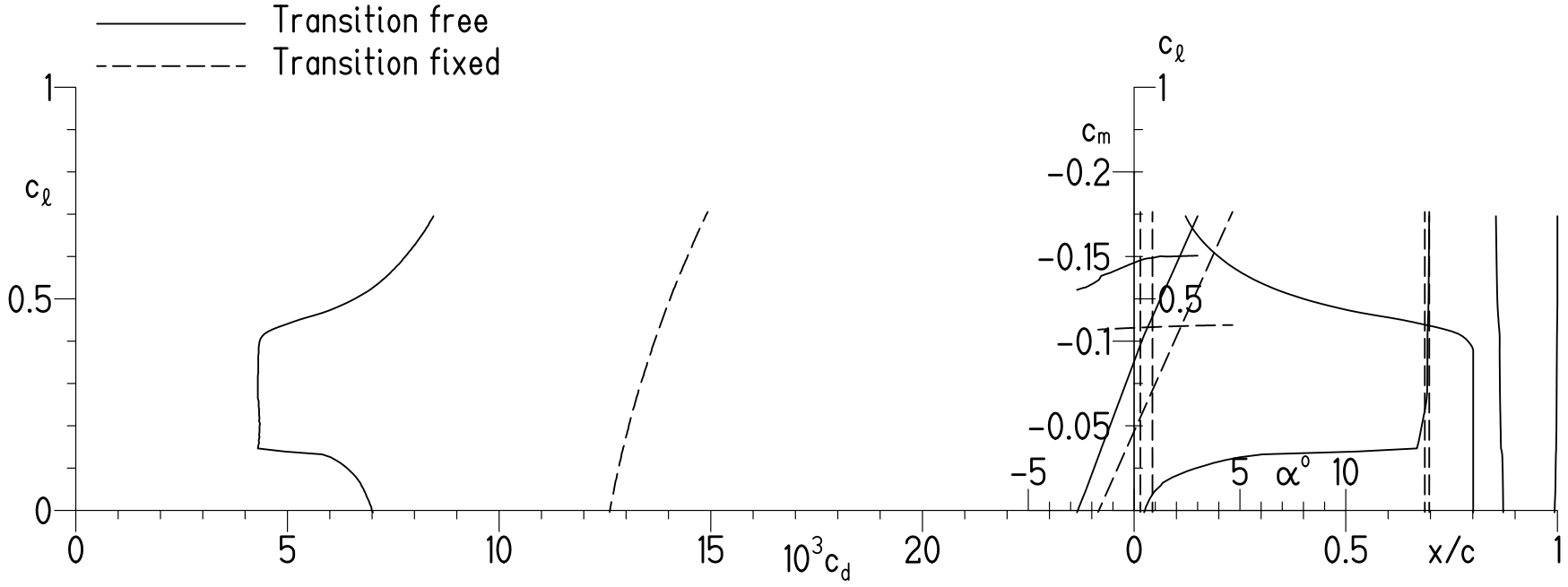

(b) $R = 6 \times 10^6$.

Figure 8.- Continued.

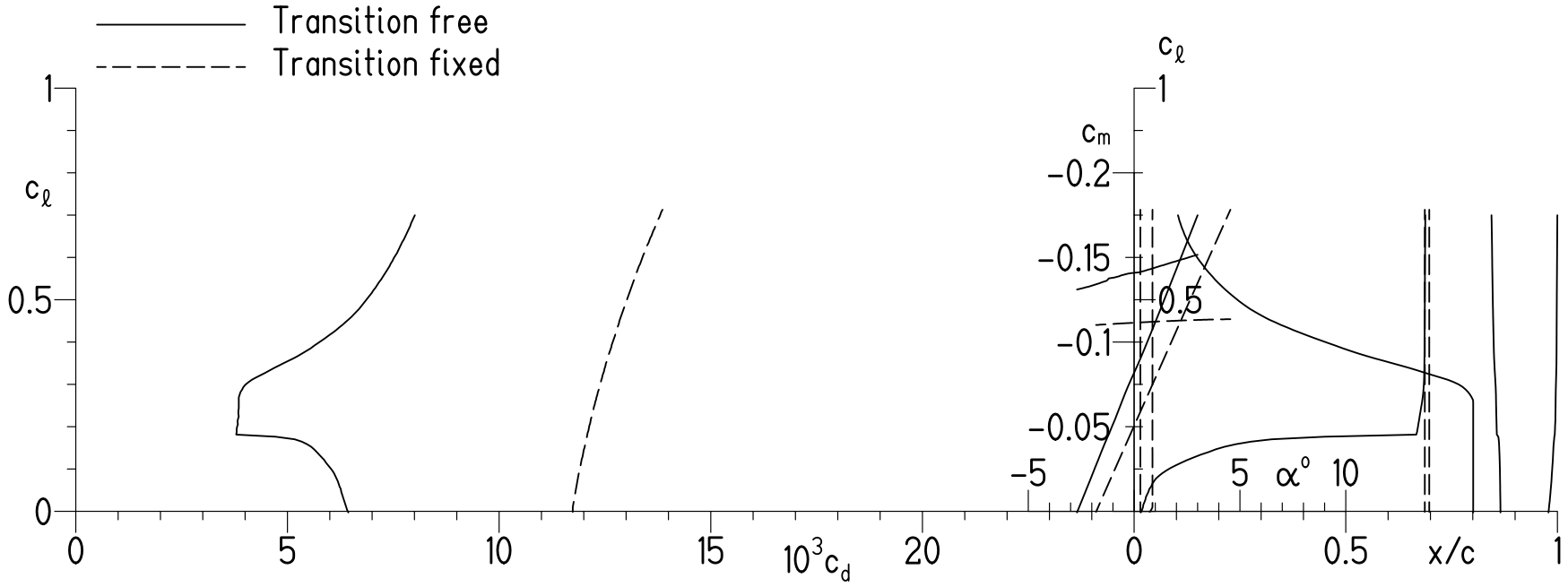

(c) $R = 9 \times 10^6$.

Figure 8.- Continued.

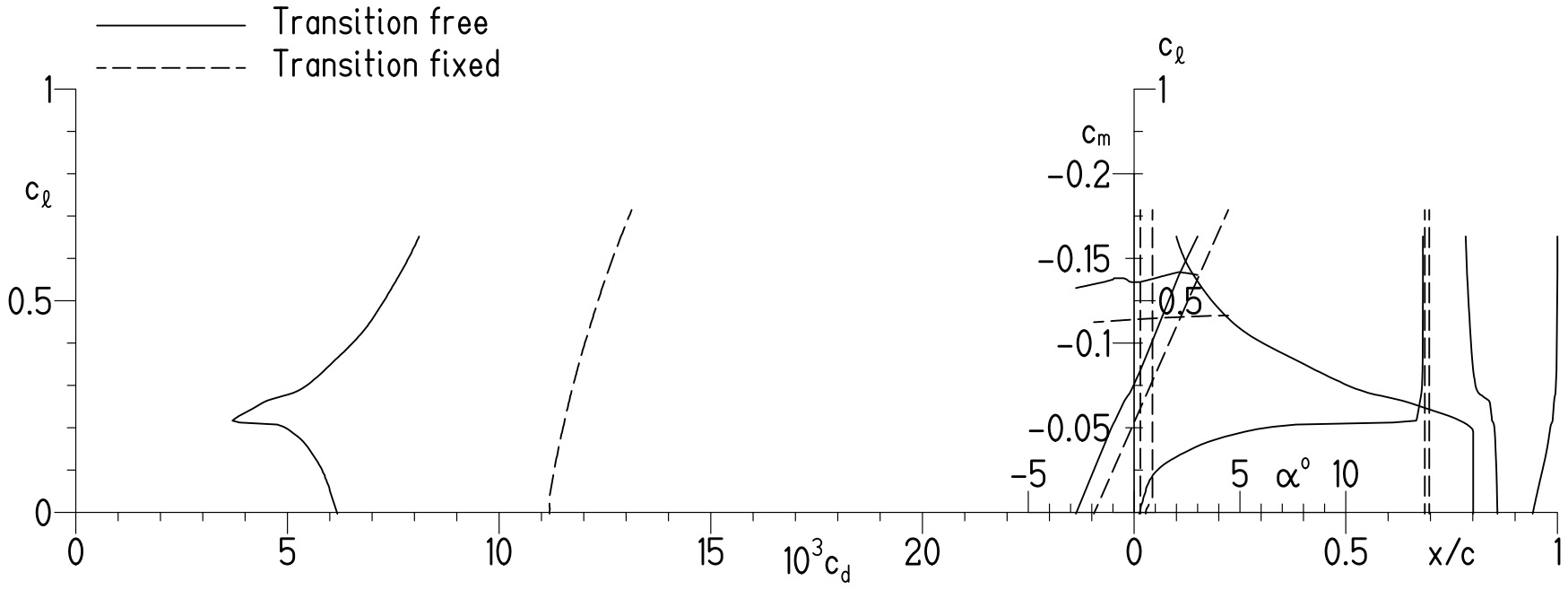

(d) $R = 12 \times 10^6$.

Figure 8.- Concluded.

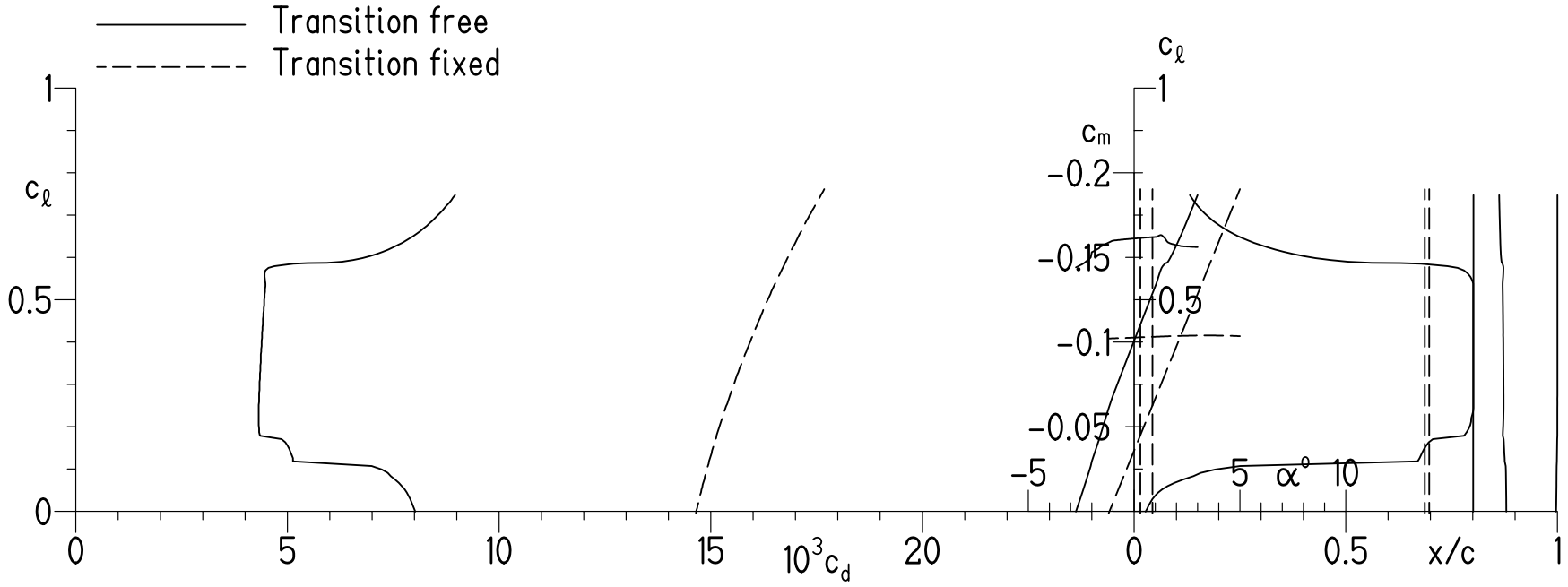

(a) $R = 4 \times 10^6$.

Figure 9.- Section characteristics at M = 0.50.

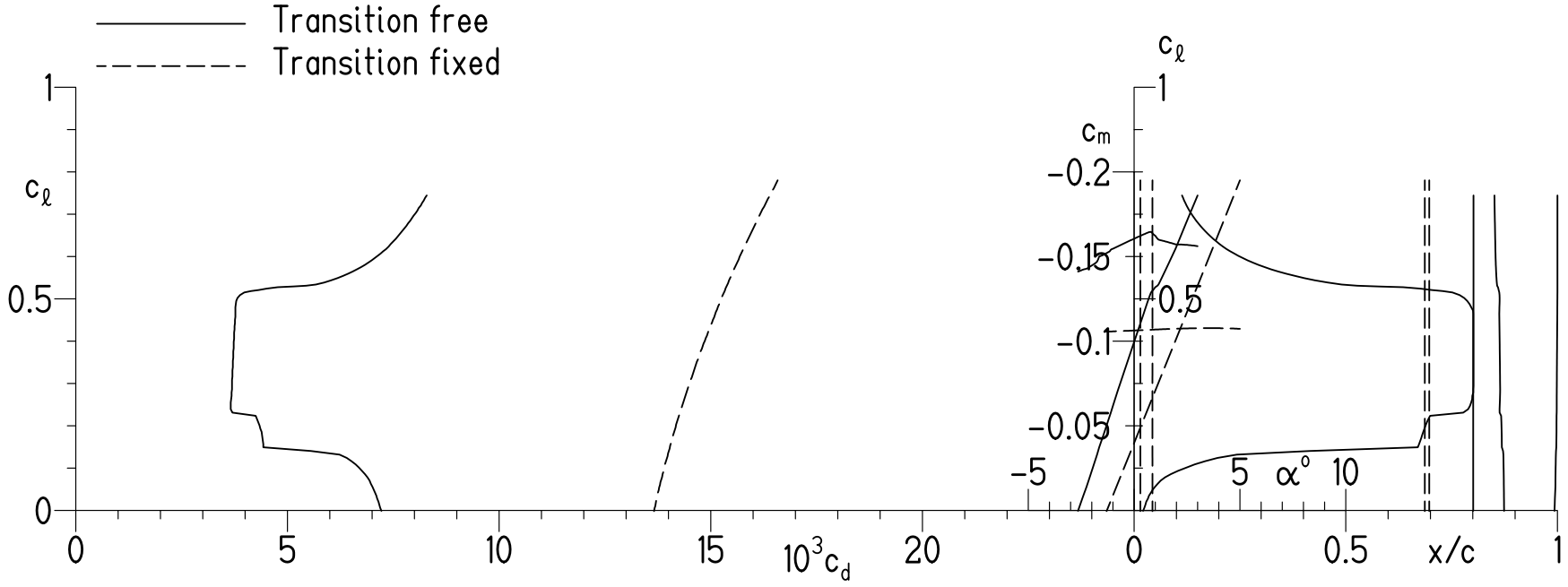

(b) $R = 6 \times 10^6$.

Figure 9.- Continued.

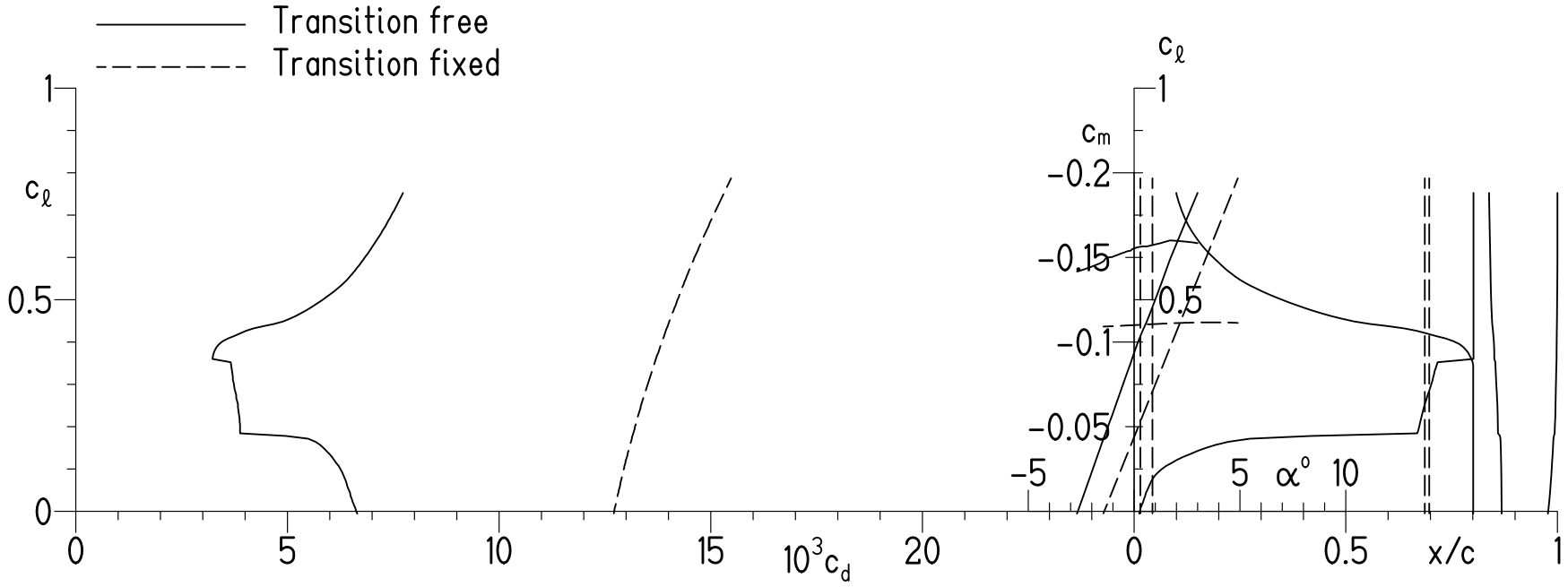

(c) $R = 9 \times 10^6$.

Figure 9.- Continued.

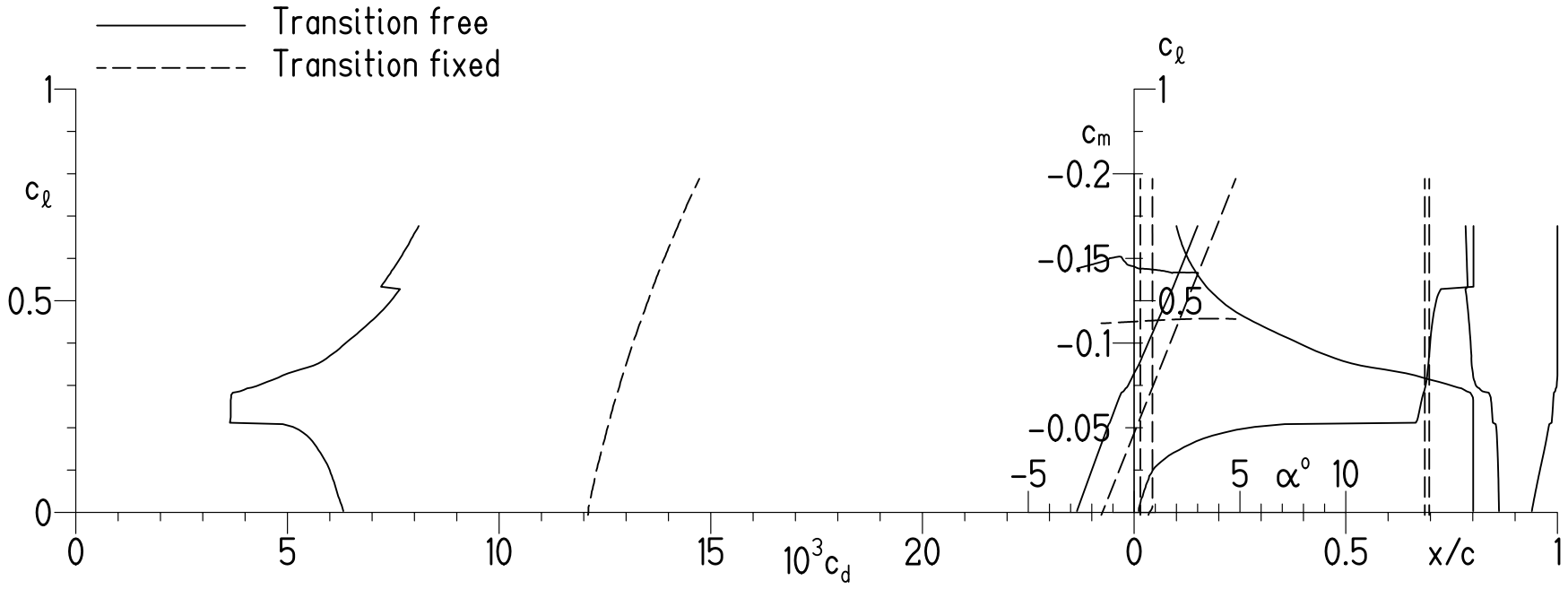

(d) $R = 12 \times 10^6$.

Figure 9.- Concluded.

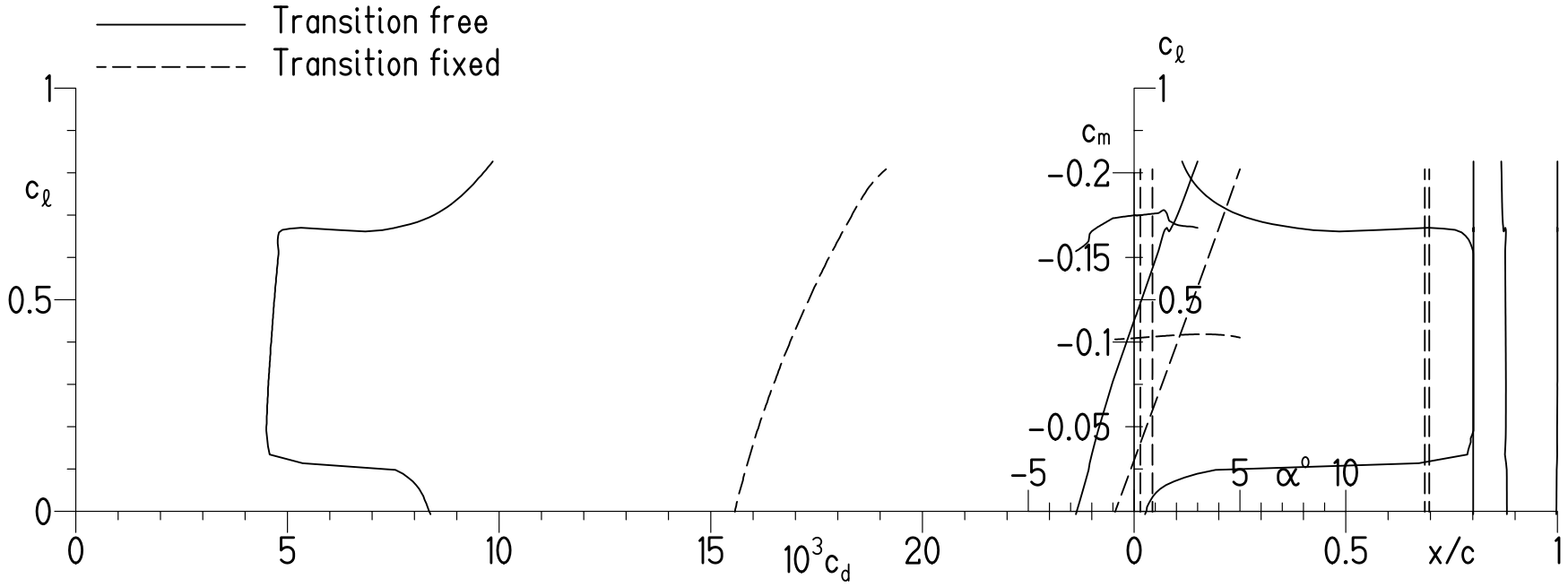

(a) $R = 4 \times 10^6$.

Figure 10.- Section characteristics at M = 0.60.

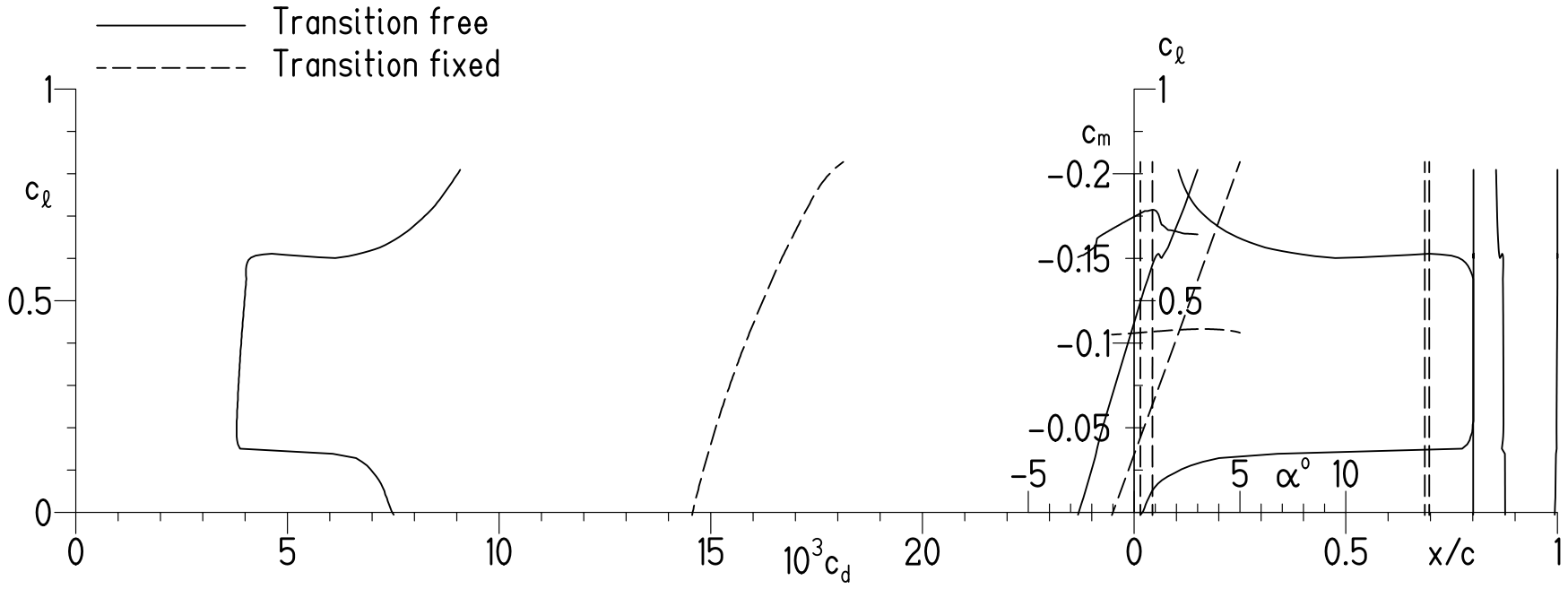

(b) $R = 6 \times 10^6$.

Figure 10.- Continued.

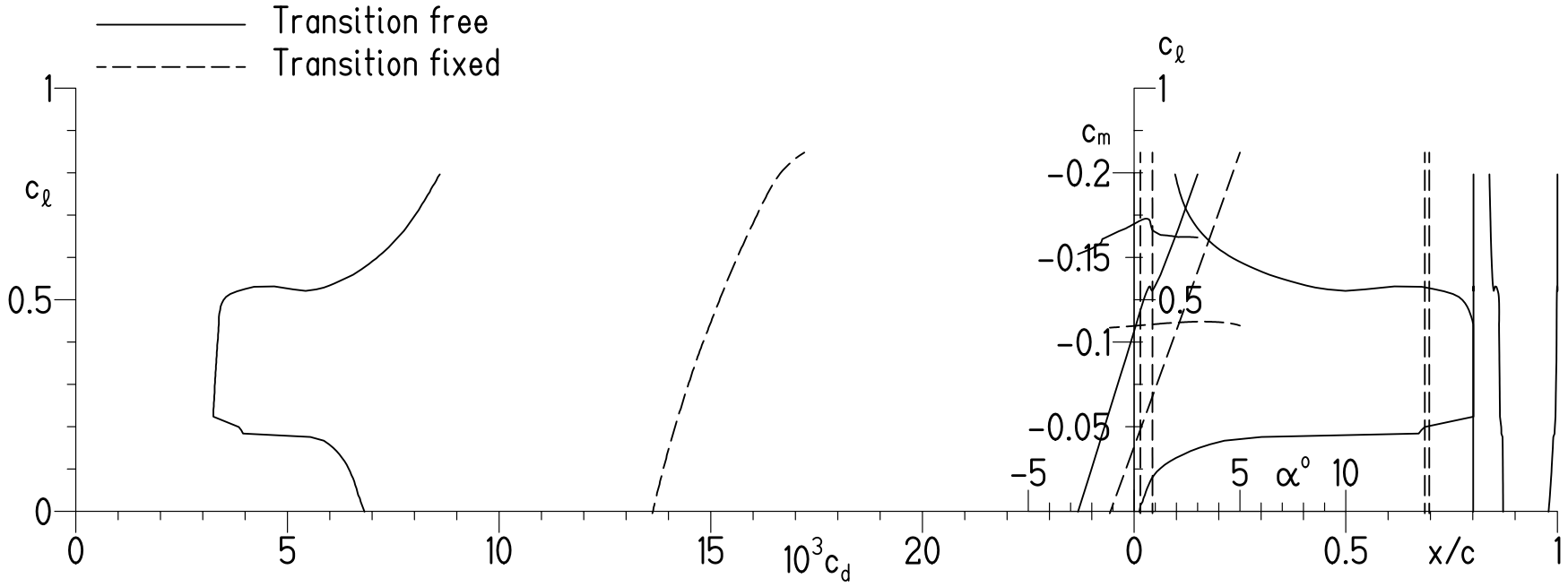

(c) $R = 9 \times 10^6$.

Figure 10.- Continued.

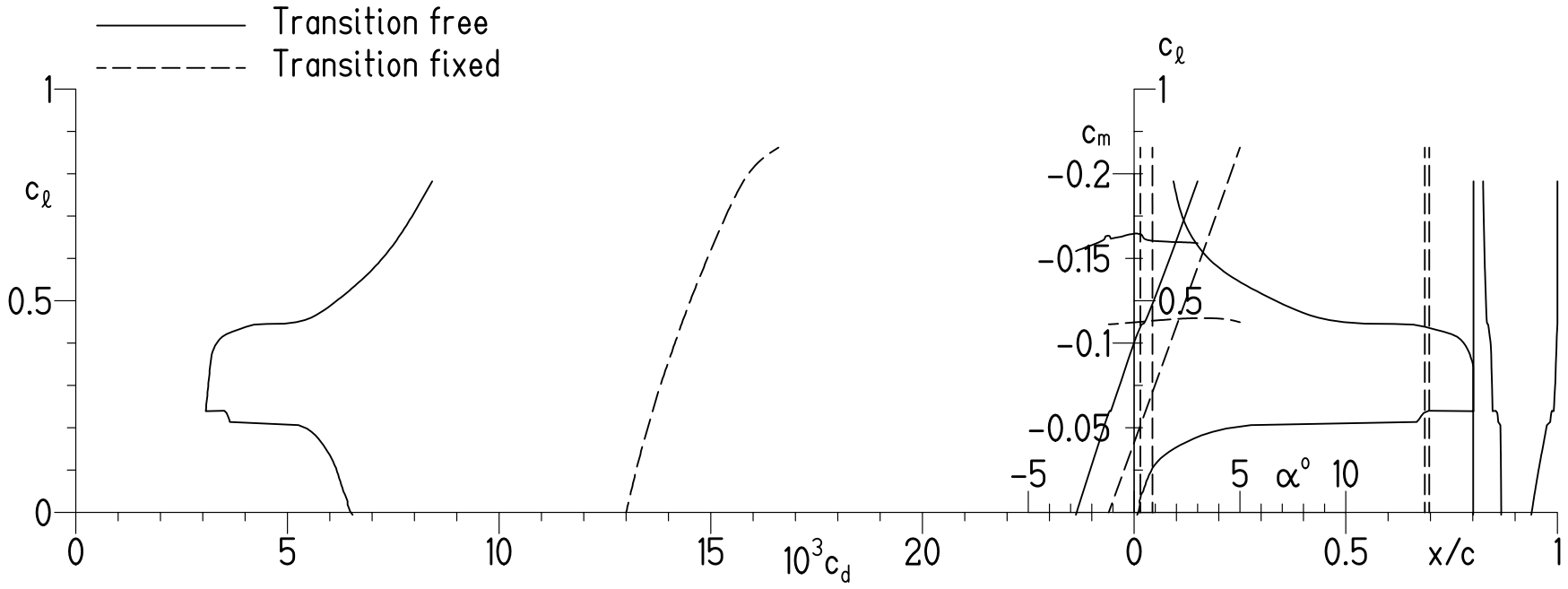

(d) $R = 12 \times 10^6$.

Figure 10.- Concluded.

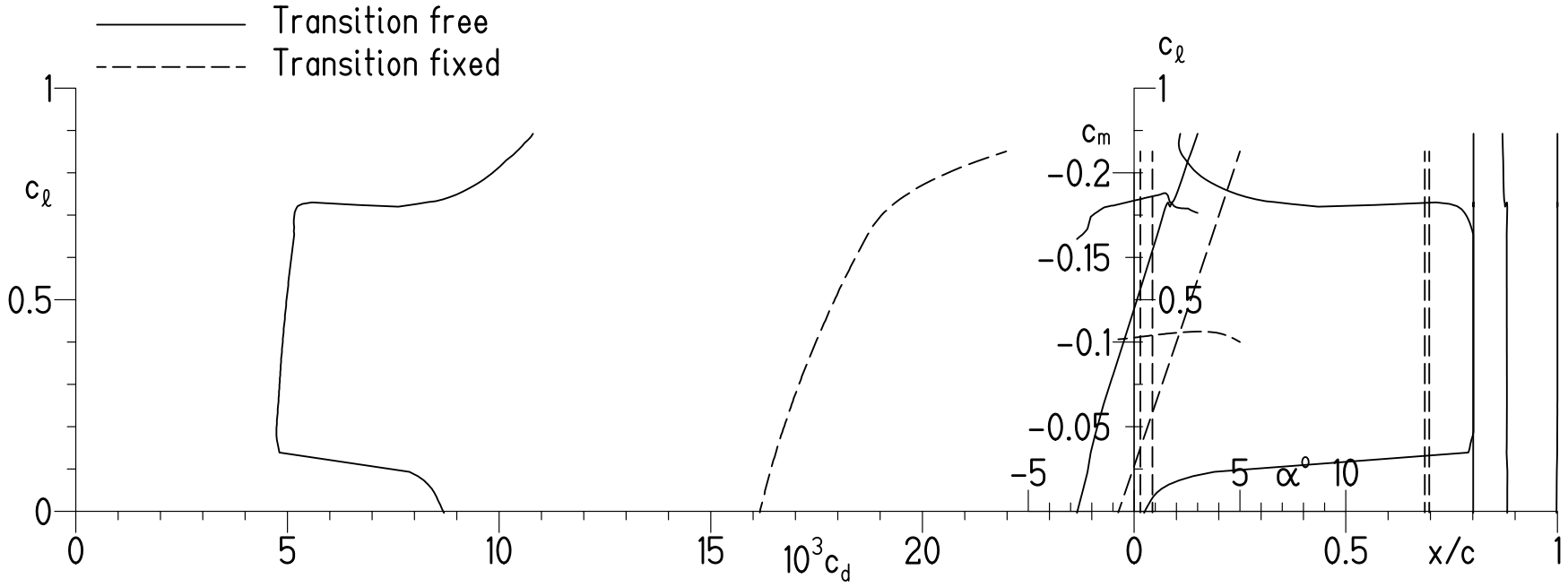

(a) $R = 4 \times 10^6$.

Figure 11.- Section characteristics at $M = 0.65$.

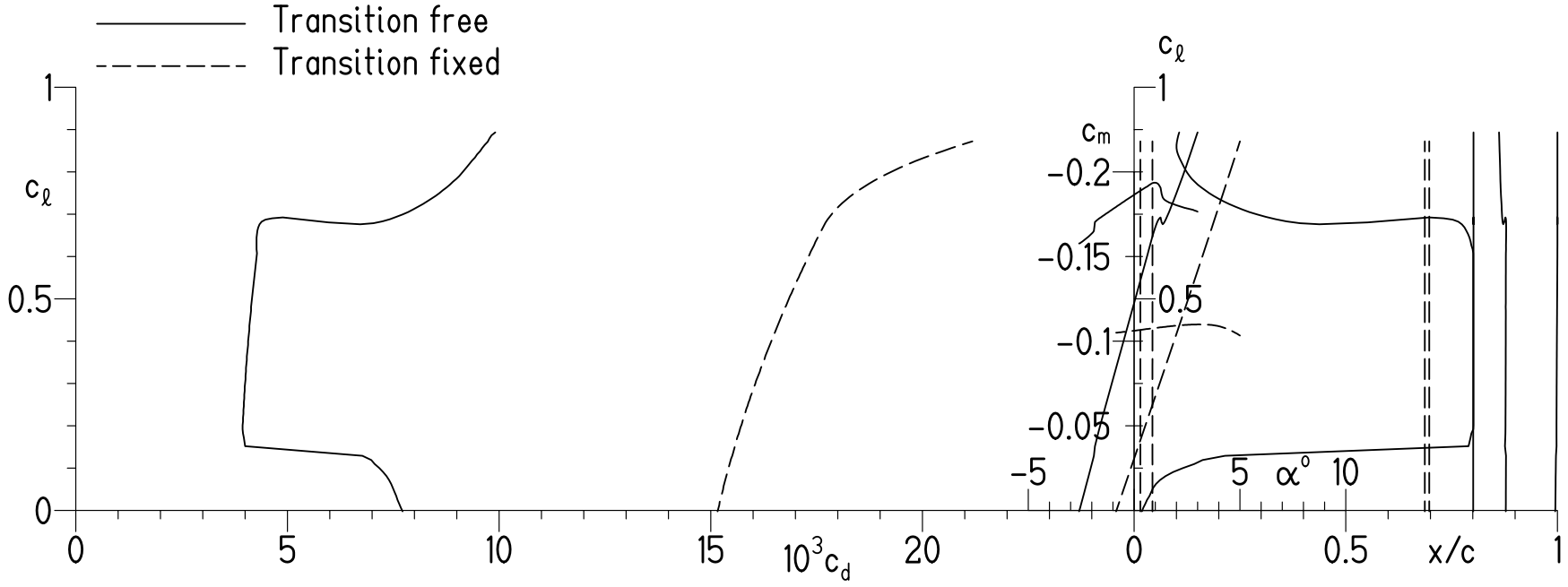

(b) $R = 6 \times 10^6$.

Figure 11.- Continued.

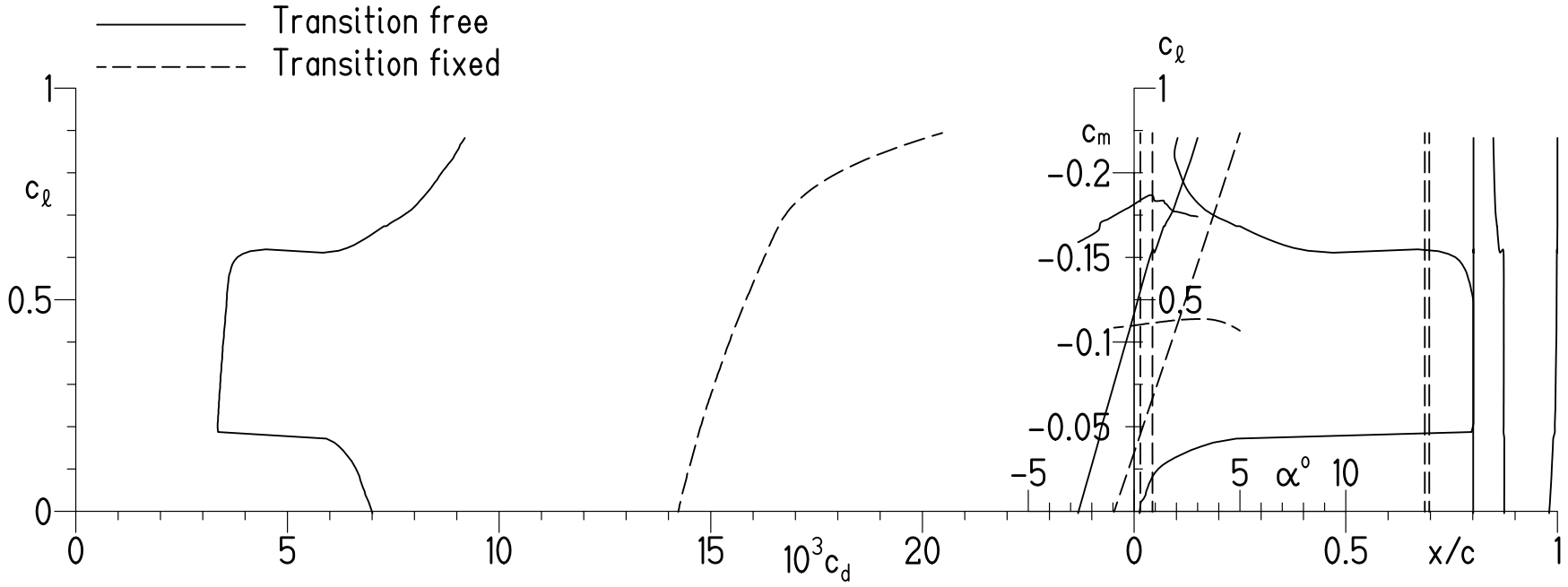

(c) $R = 9 \times 10^6$.

Figure 11.- Continued.

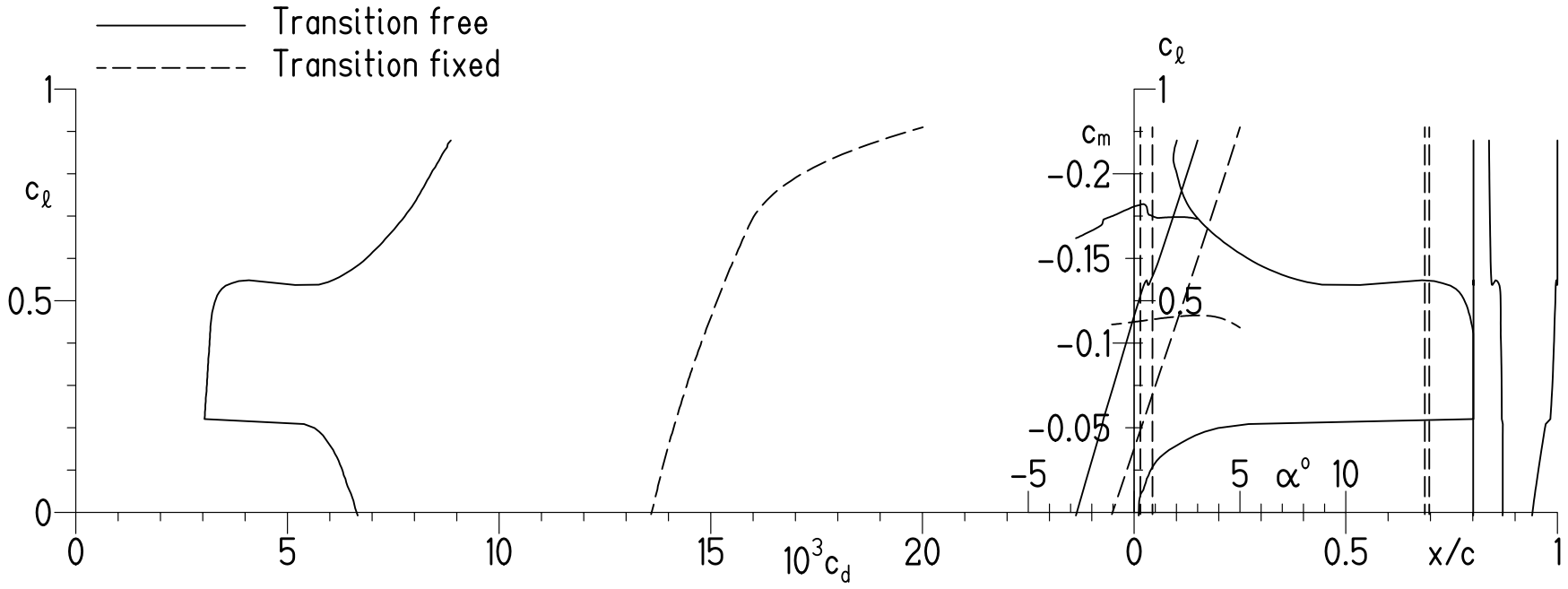

(d) $R = 12 \times 10^6$.

Figure 11.- Concluded.

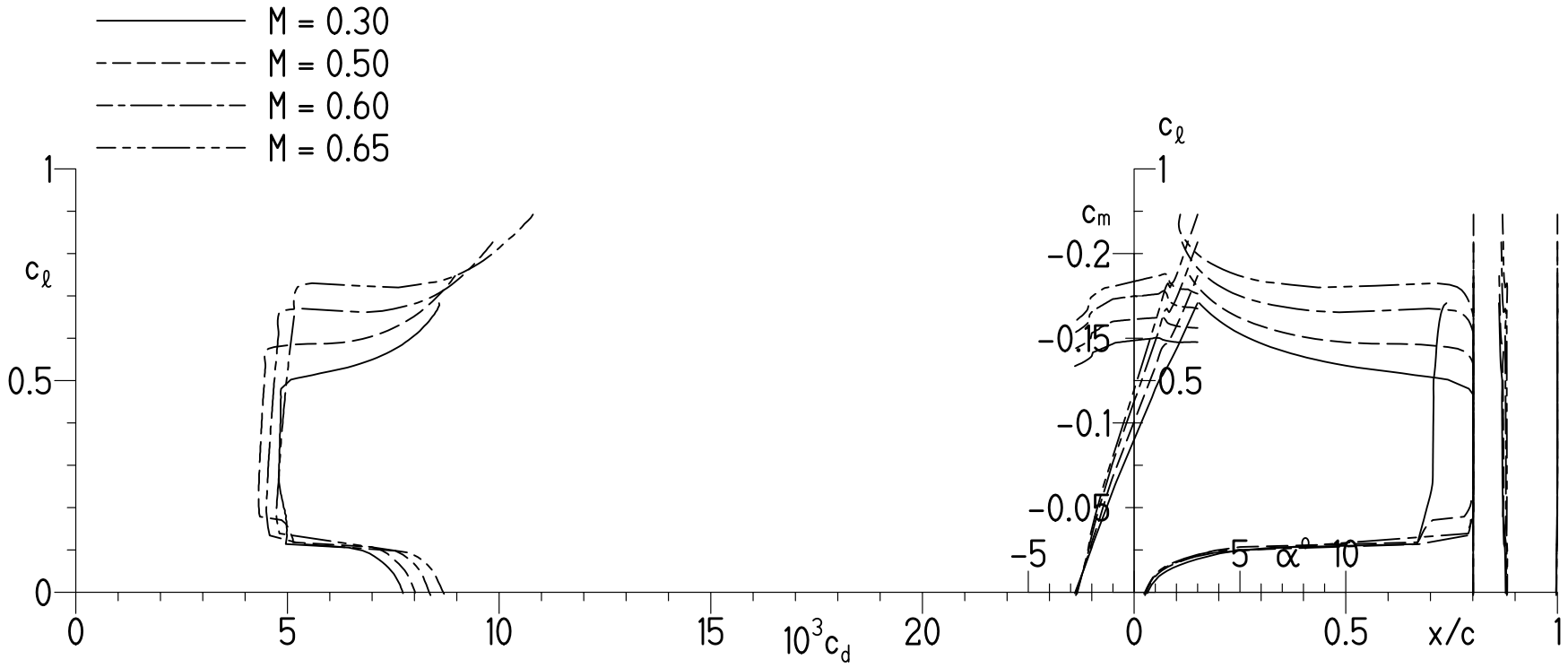

(a) $R = 4 \times 10^6$.

Figure 12.- Effect of Mach number on section characteristics with transition free.

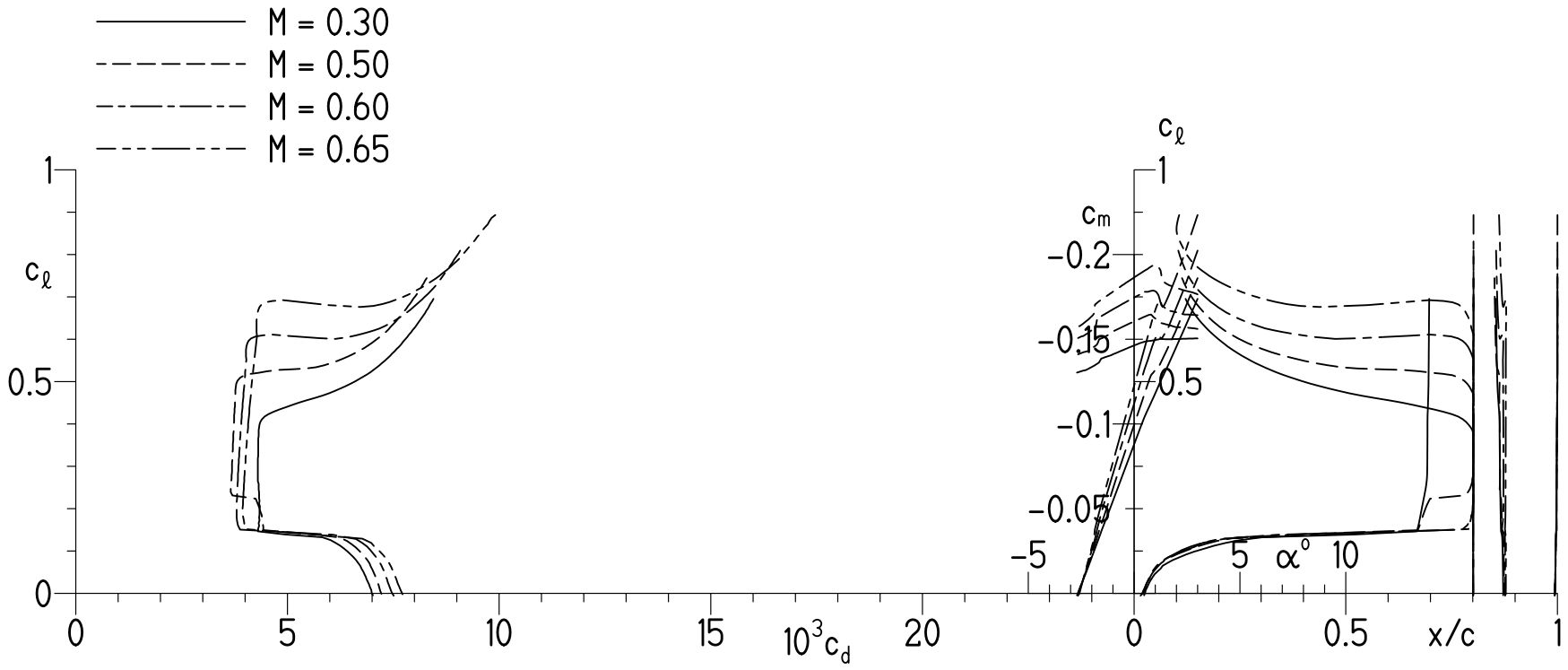

(b) $R = 6 \times 10^6$.

Figure 12.- Continued.

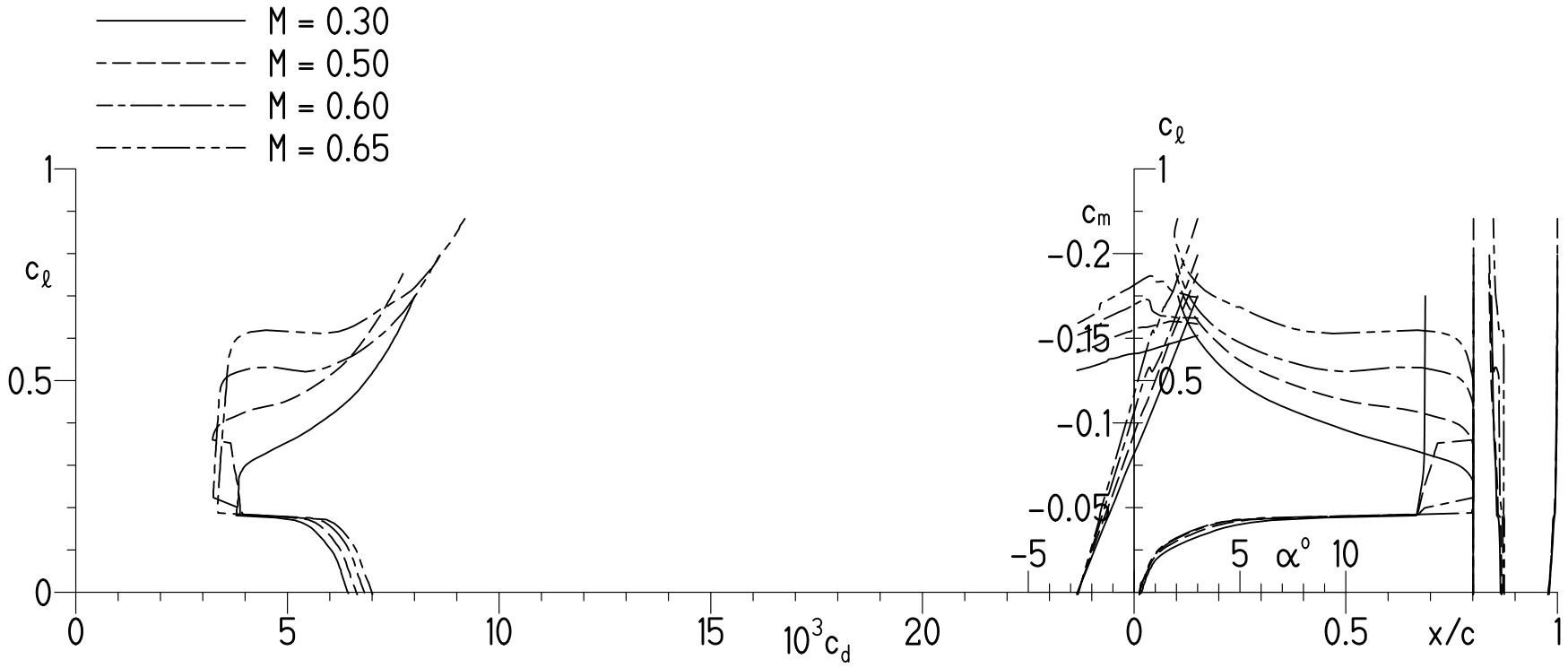

(c) $R = 9 \times 10^6$.

Figure 12.- Continued.

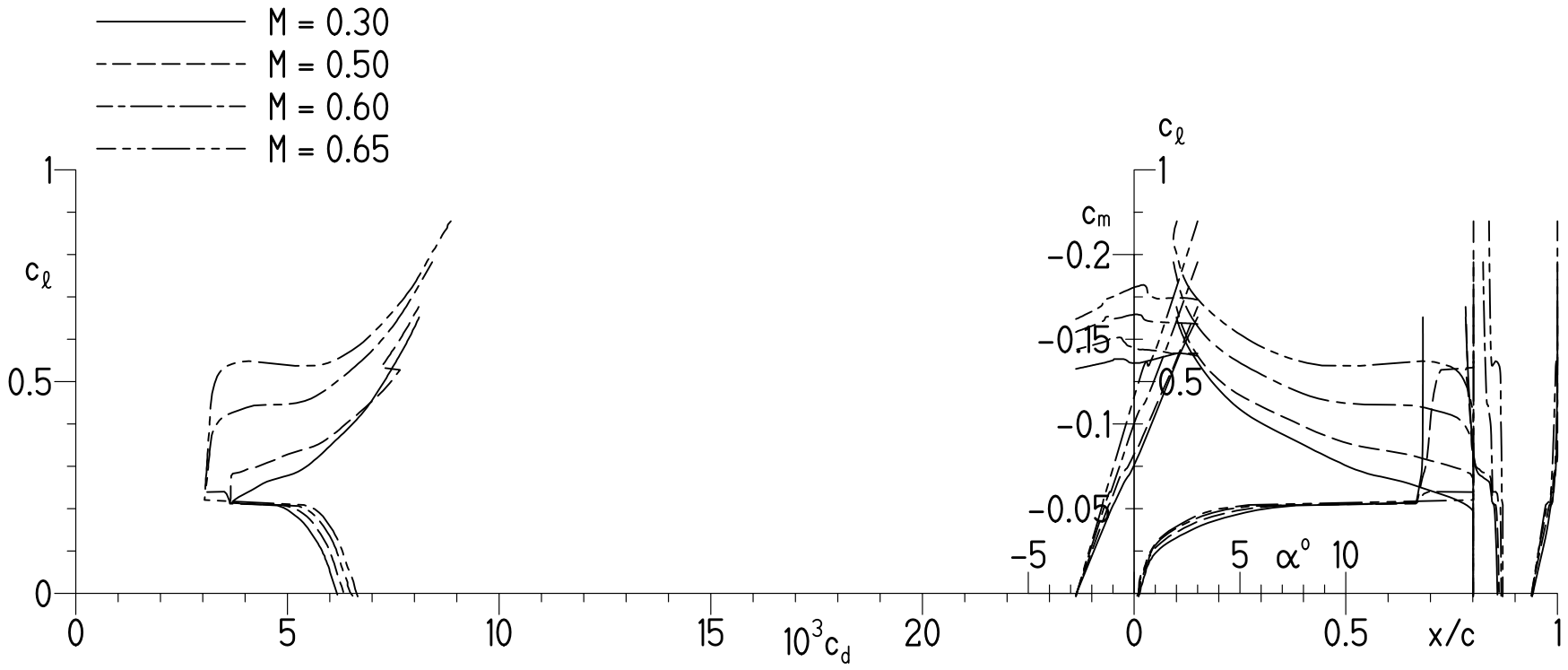

(d) $R = 12 \times 10^6$.

Figure 12.- Concluded.

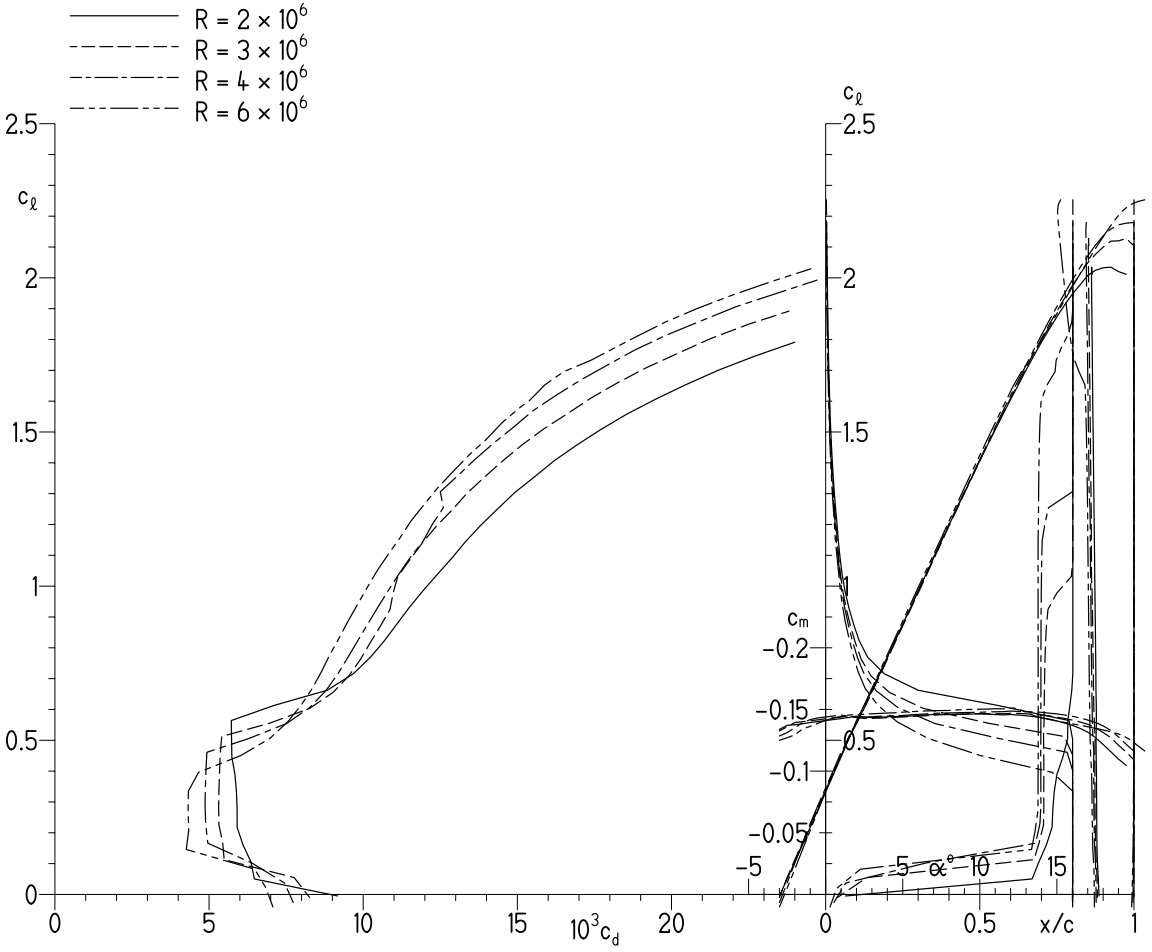

(a) M = 0.10.

Figure 13.- Effect of Reynolds number on section characteristics with transition free.

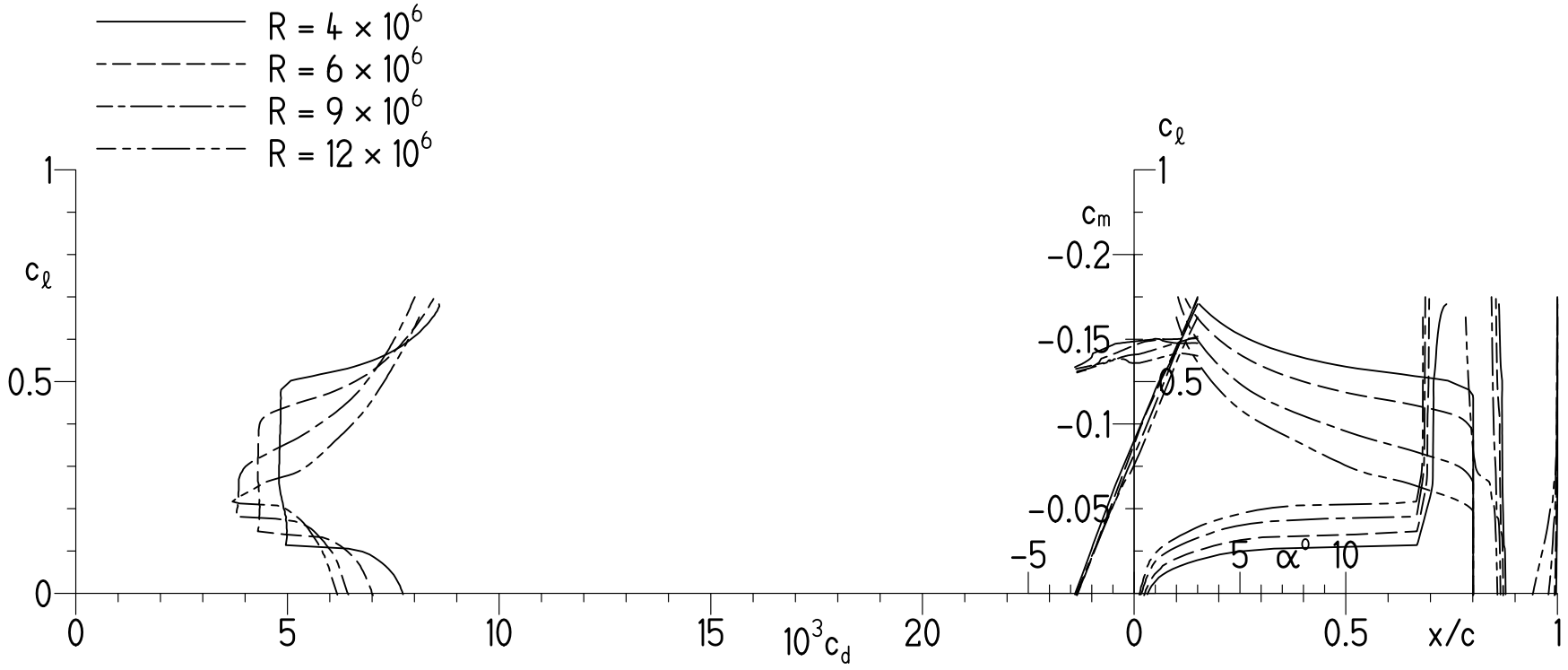

(b) M = 0.30.

Figure 13.- Continued.

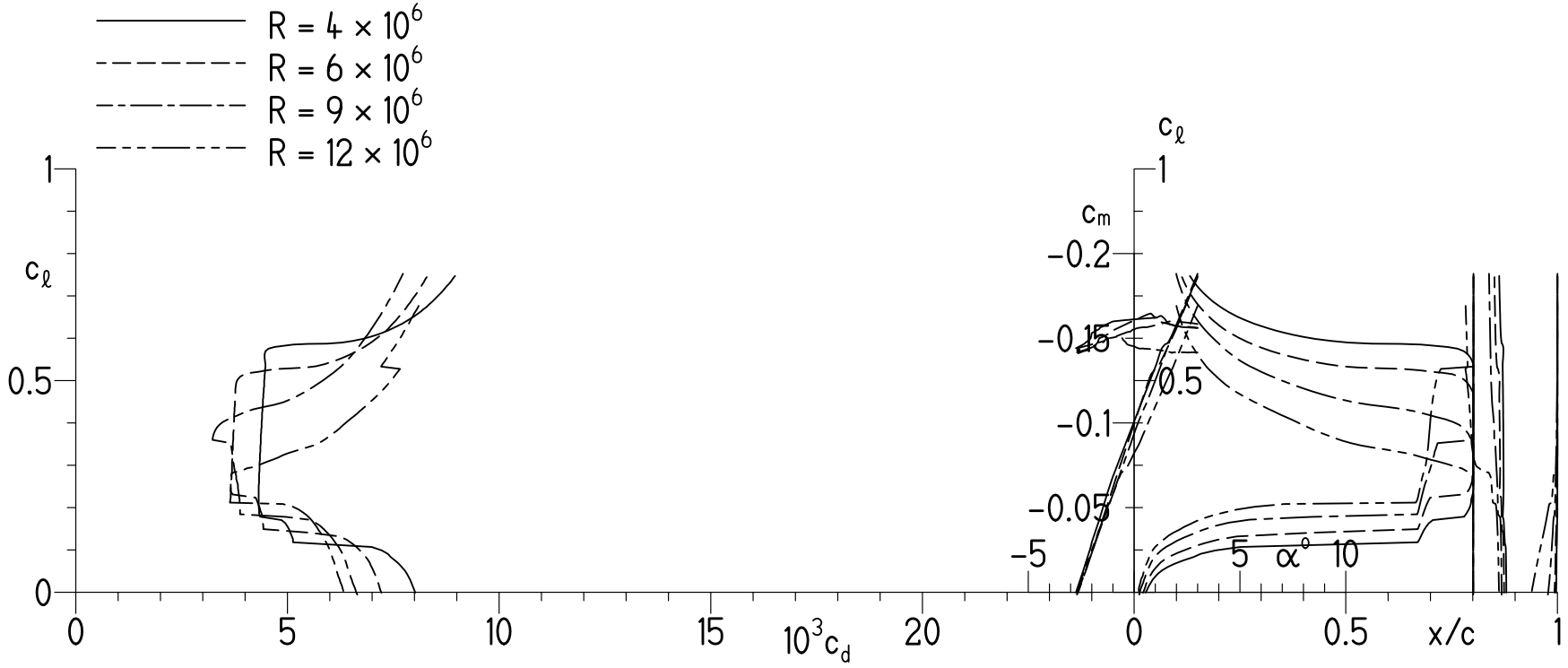

(c) M = 0.50.

Figure 13.- Continued.

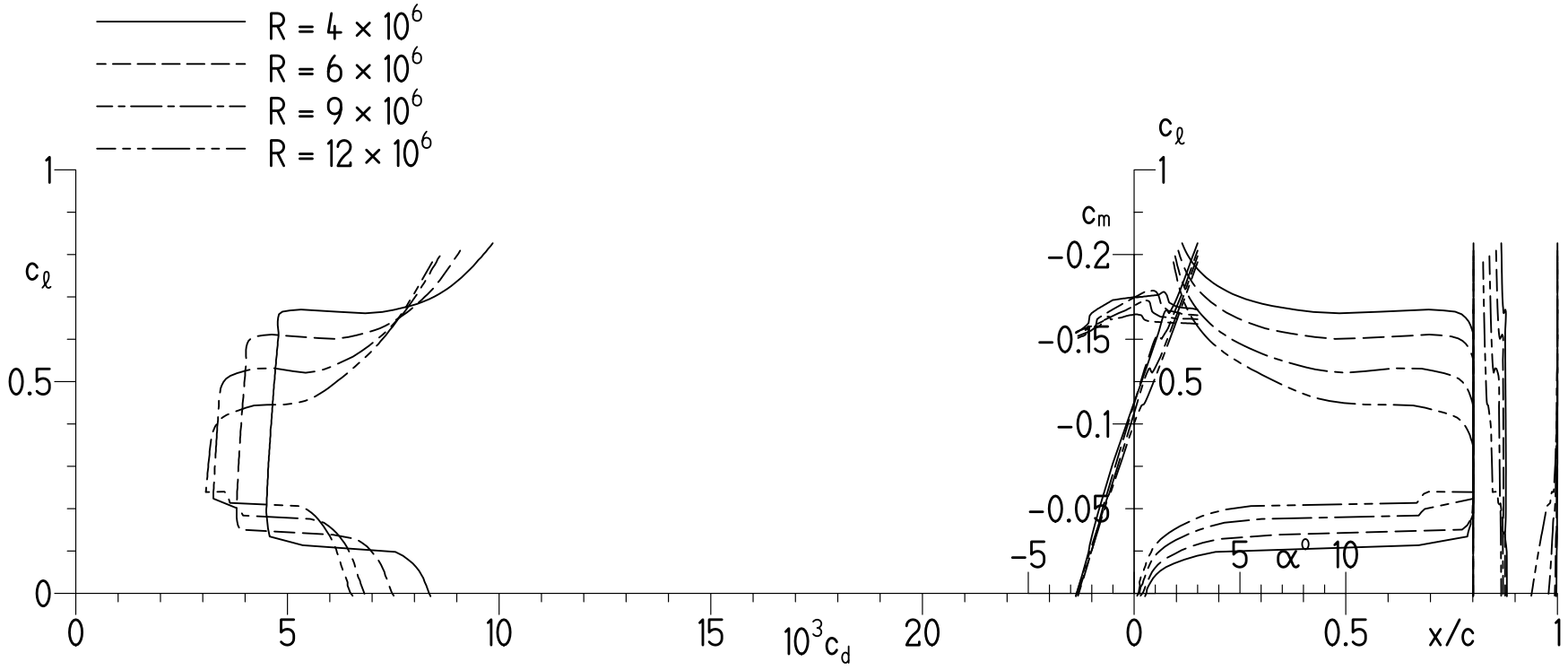

(d) M = 0.60.

Figure 13.- Continued.

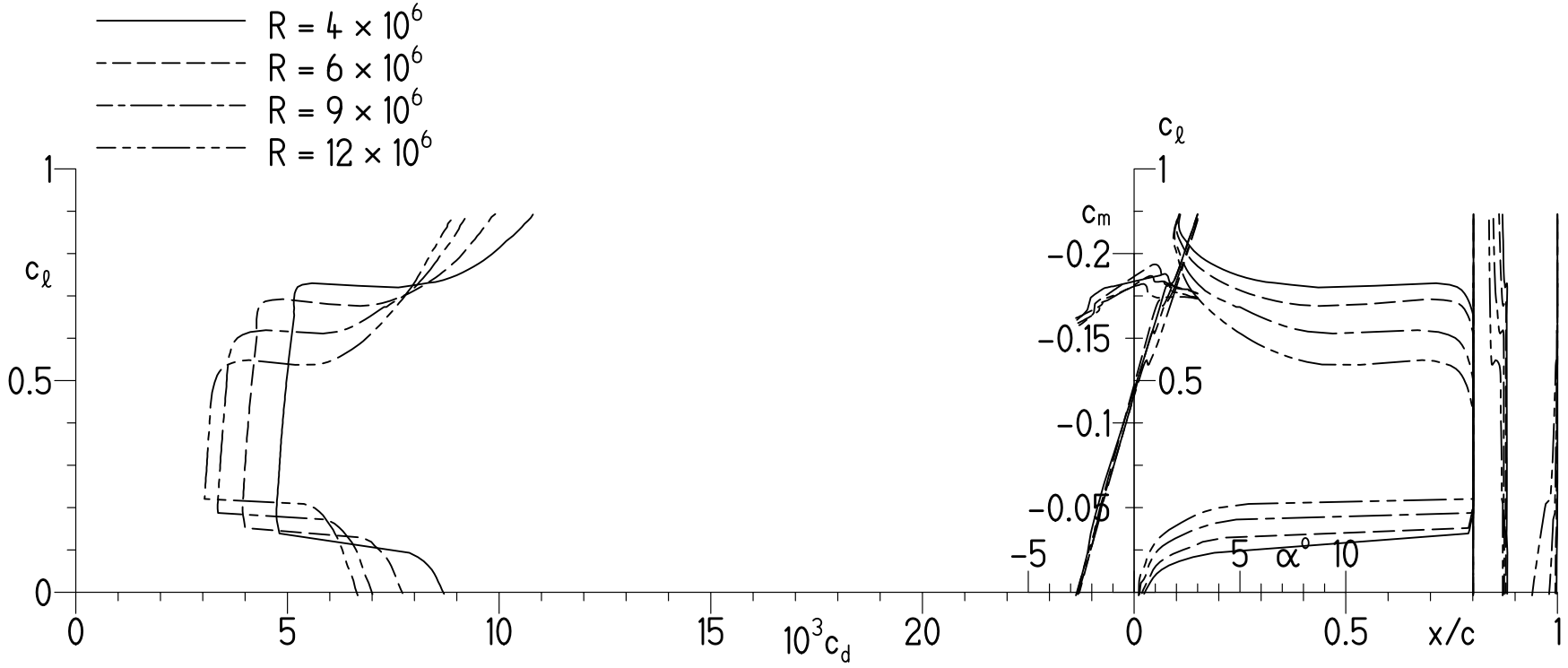

(e) M = 0.65.

Figure 13.- Concluded.

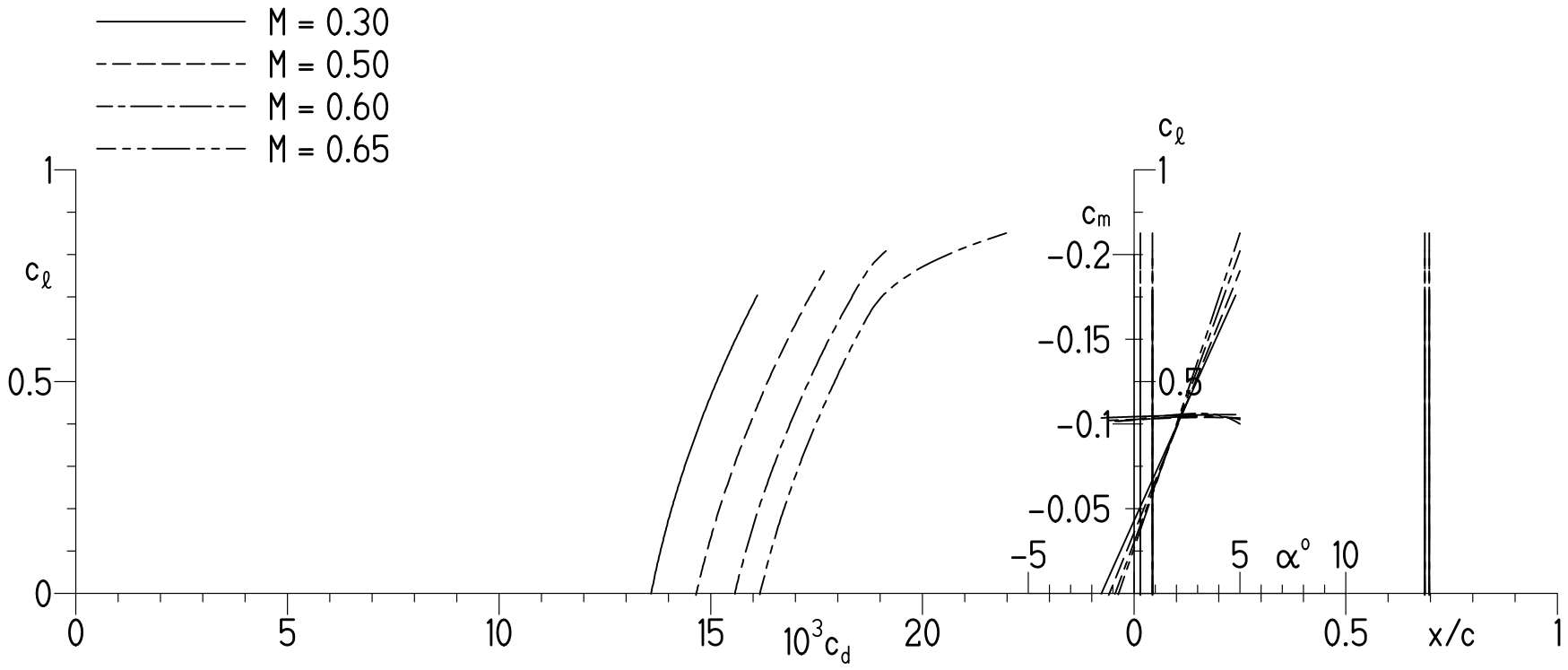

(a) $R = 4 \times 10^6$.

Figure 14.- Effect of Mach number on section characteristics with transition fixed.

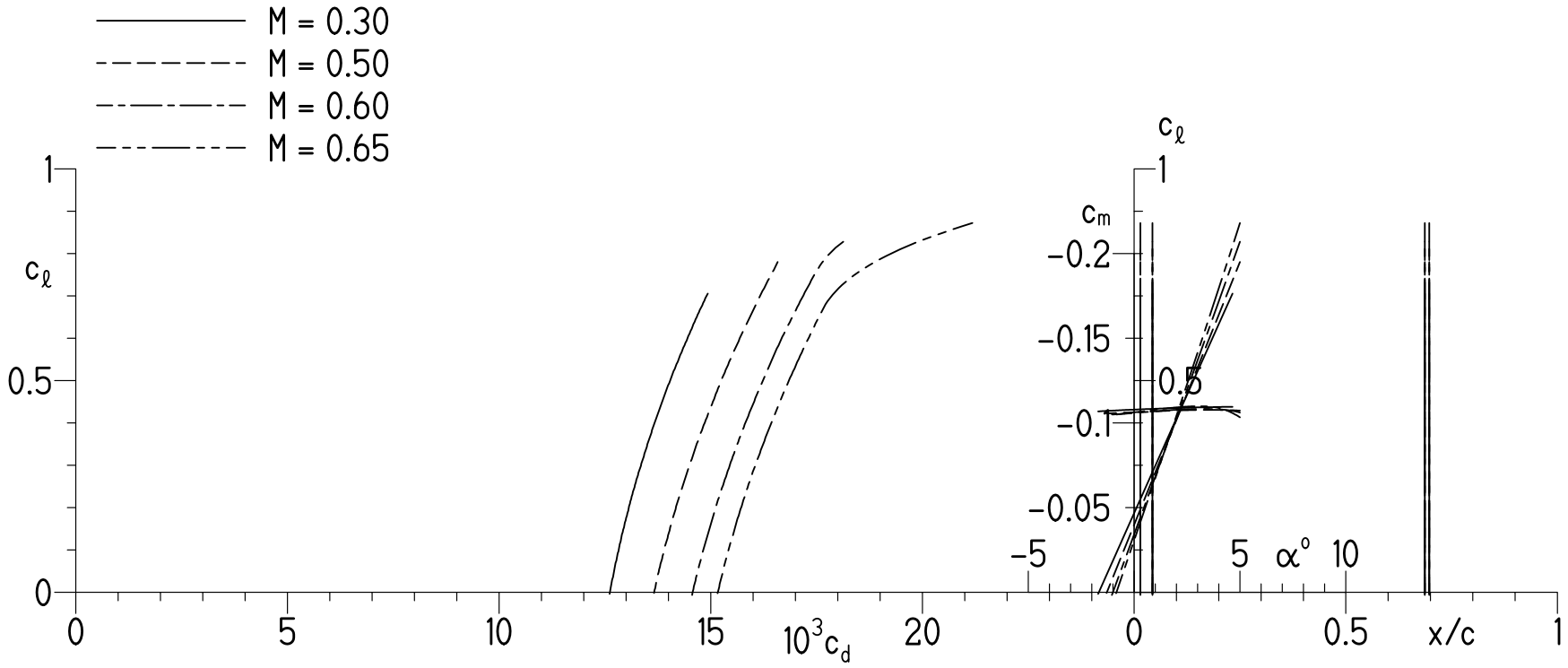

(b) $R = 6 \times 10^6$.

Figure 14.- Continued.

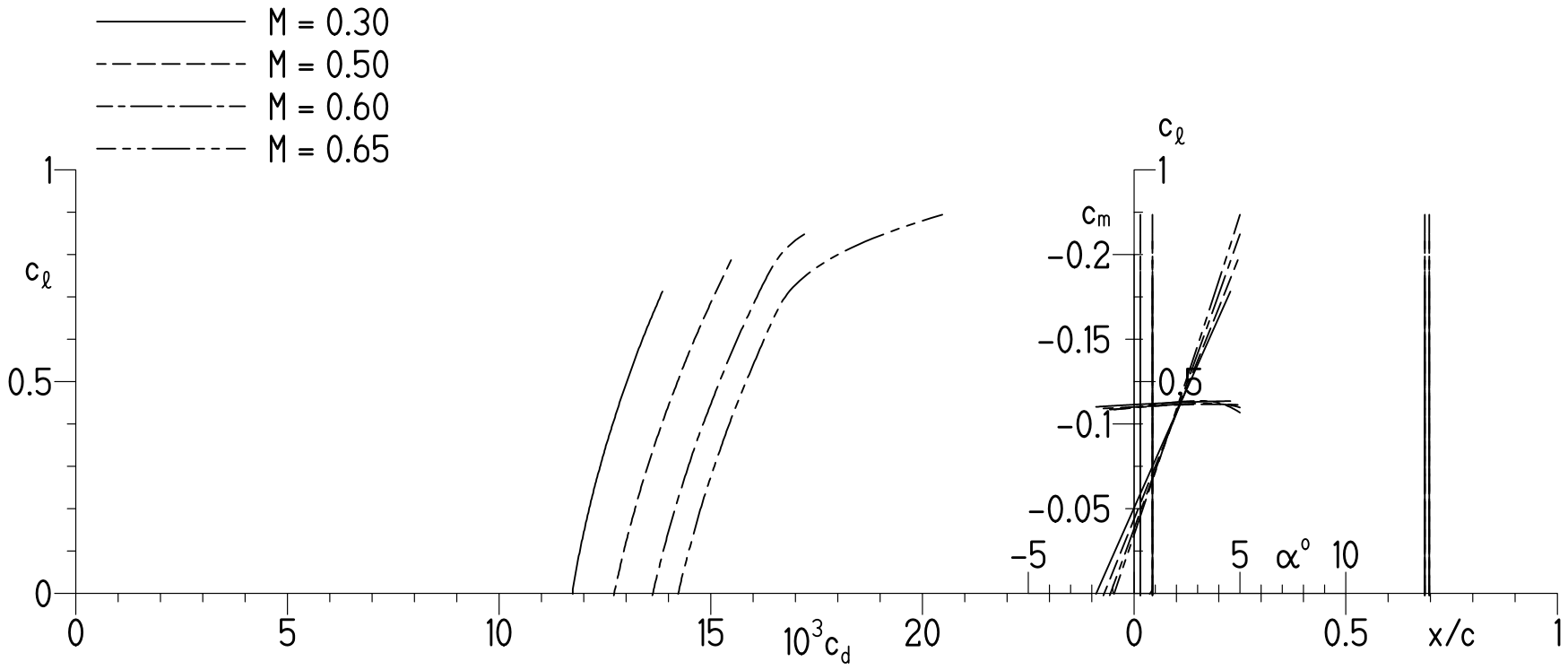

(c) $R = 9 \times 10^6$.

Figure 14.- Continued.

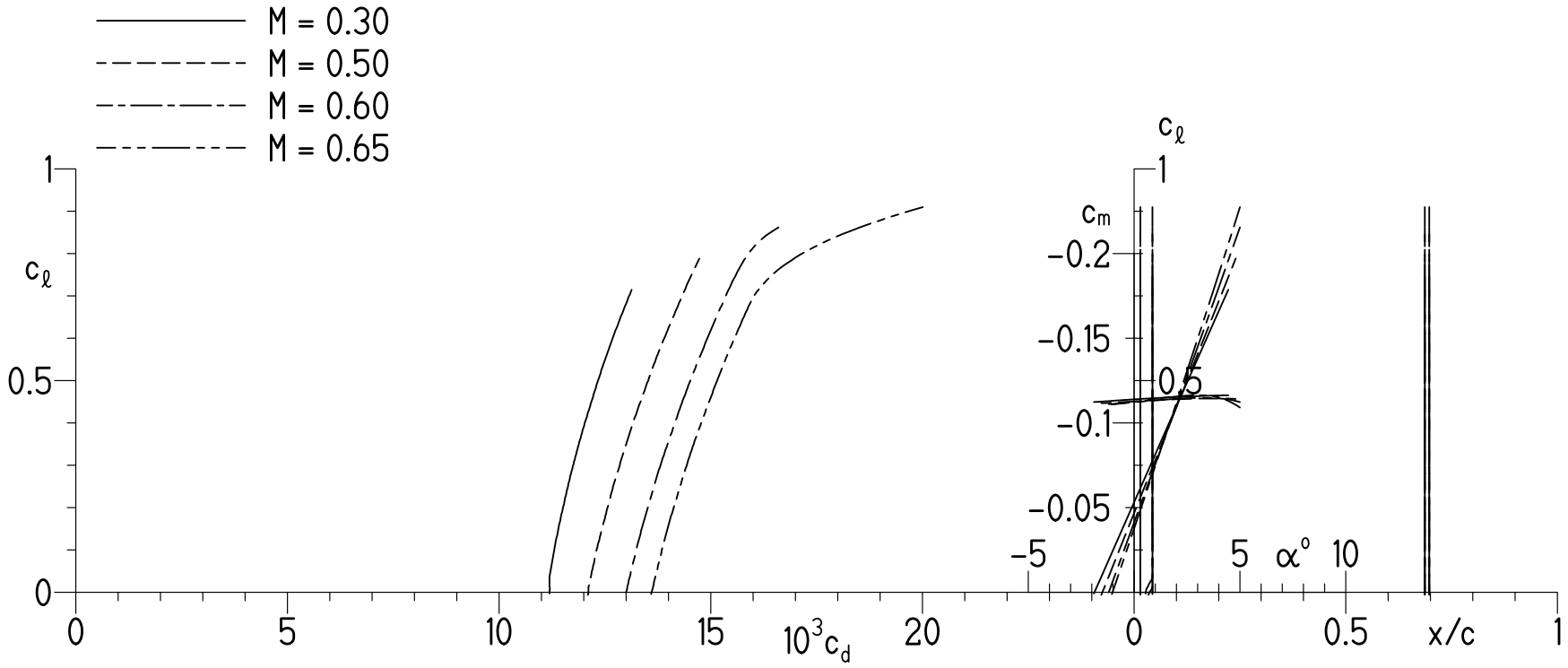

(d) $R = 12 \times 10^6$.

Figure 14.- Concluded.

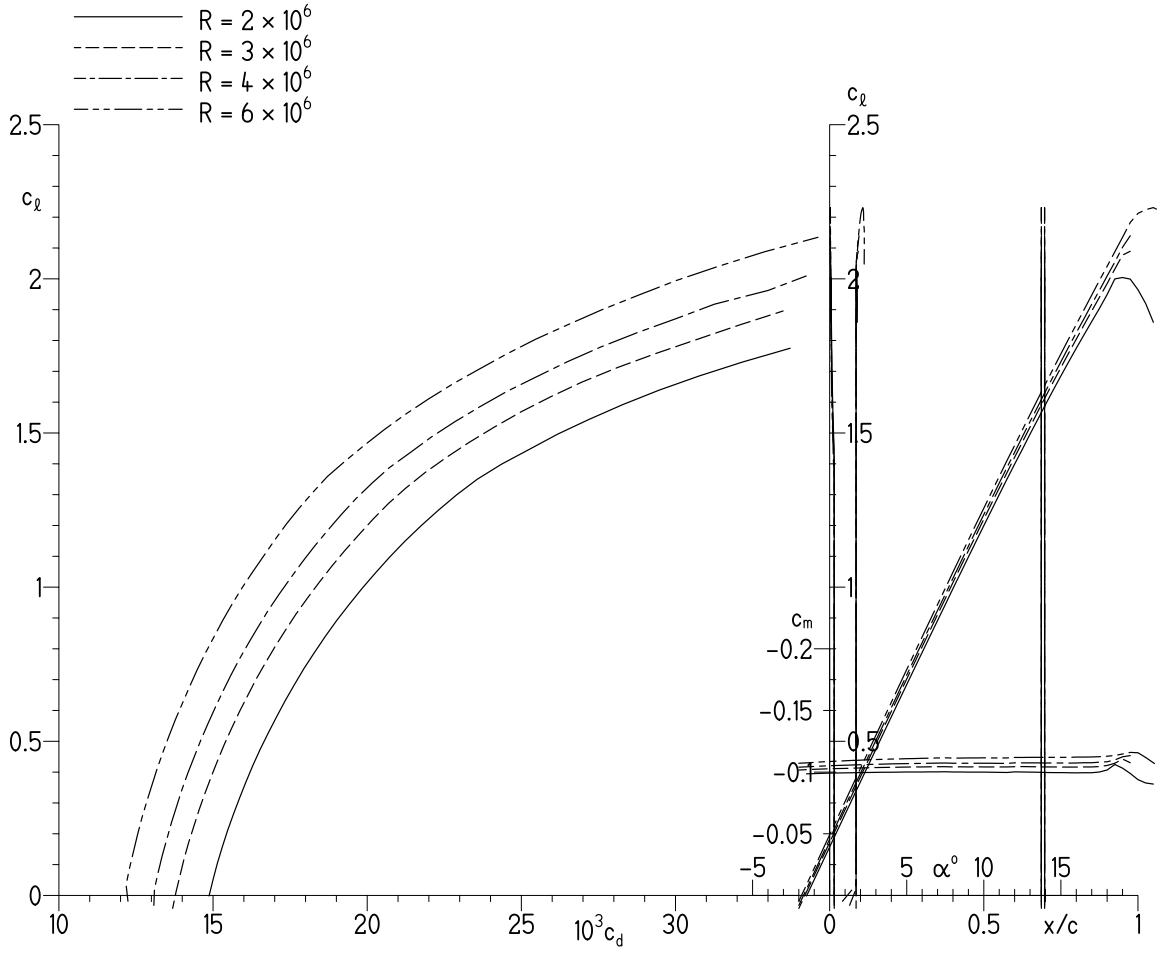

(a) M = 0.10.

Figure 15.- Effect of Reynolds number on section characteristics with transition fixed.

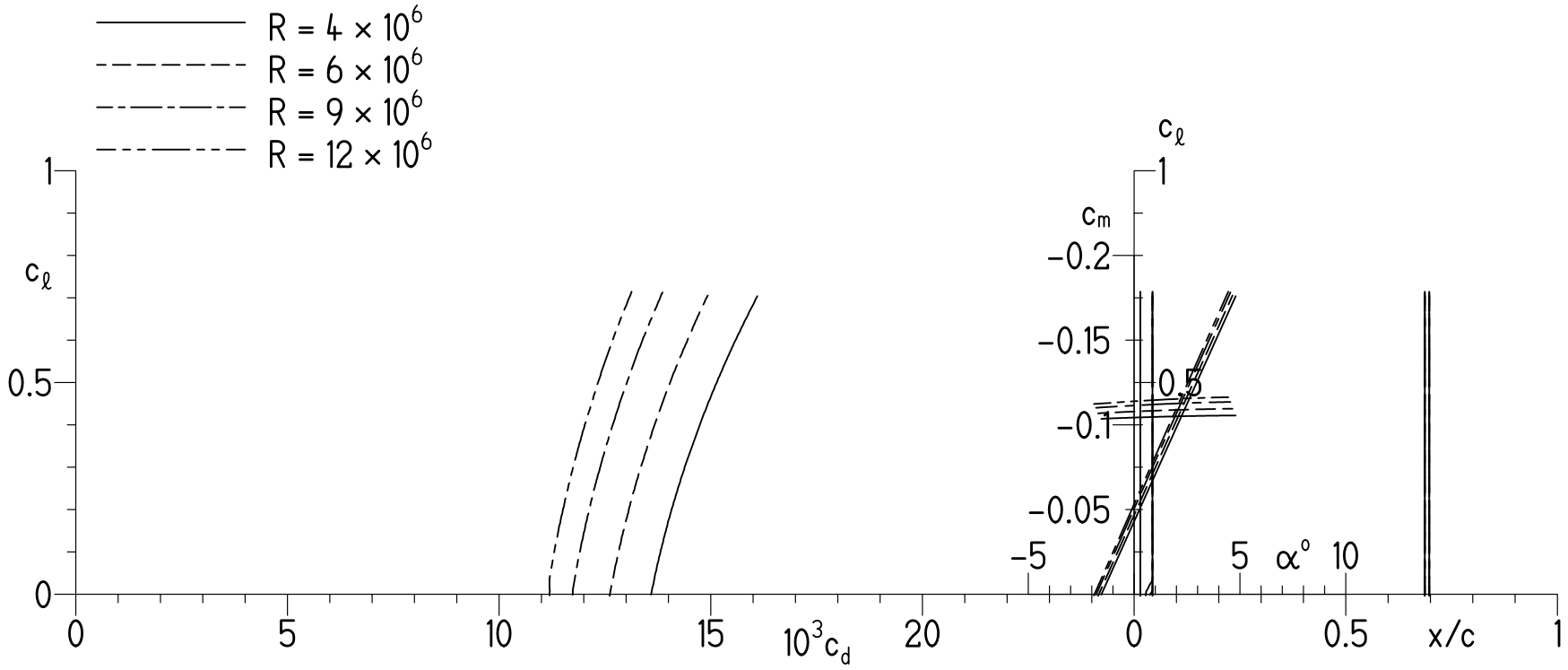

(b) M = 0.30.

Figure 15.- Continued.

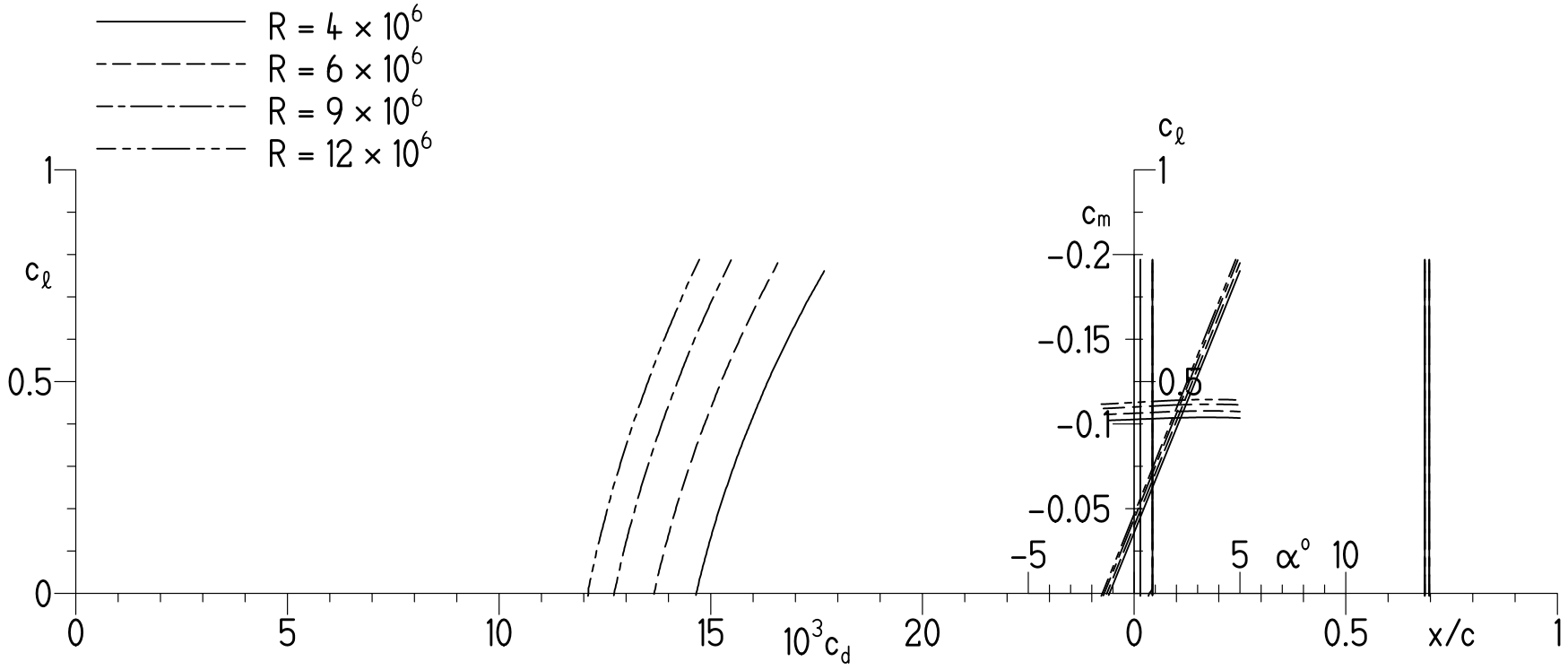

(c) M = 0.50.

Figure 15.- Continued.

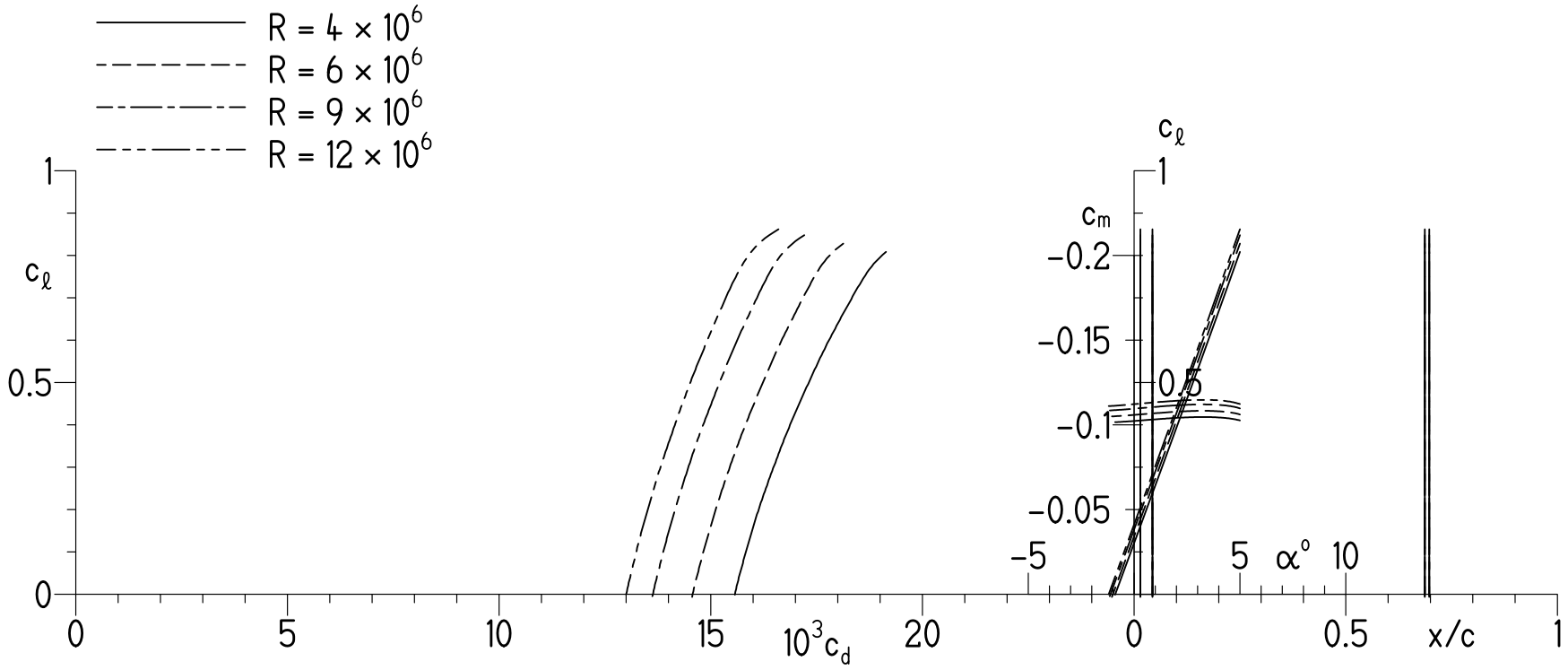

(d) M = 0.60.

Figure 15.- Continued.

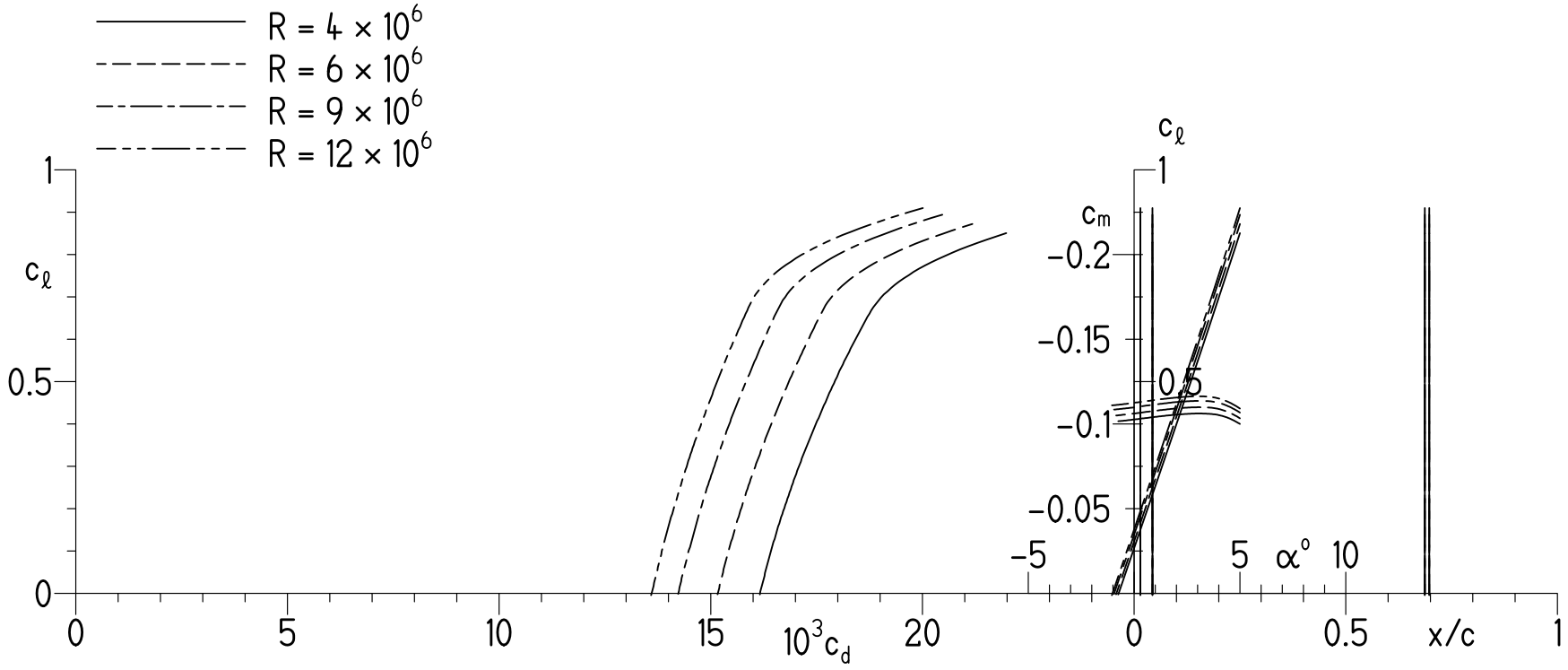

(e) M = 0.65.

Figure 15.- Concluded.

REPORT DOCUMENTATION PAGE

Form Approved
OMB No. 0704-0188

1. REPORT DATE *(DD-MM-YYYY)*	2. REPORT TYPE	3. DATES COVERED *(From - To)*
01- 07 - 2012	Contractor Report	

4. TITLE AND SUBTITLE

Design of a Slotted, Natural-Laminar-Flow Airfoil for Business-Jet Applications

5a. CONTRACT NUMBER

NNL04AD45P

5b. GRANT NUMBER

5c. PROGRAM ELEMENT NUMBER

6. AUTHOR(S)

Somers, Dan M.

5d. PROJECT NUMBER

5e. TASK NUMBER

5f. WORK UNIT NUMBER

561581.02.08.07.46.04

7. PERFORMING ORGANIZATION NAME(S) AND ADDRESS(ES)

NASA Langley Research Center
Hampton, Virginia 23681-2199

8. PERFORMING ORGANIZATION REPORT NUMBER

9. SPONSORING/MONITORING AGENCY NAME(S) AND ADDRESS(ES)

National Aeronautics and Space Administration
Washington, DC 20546-0001

10. SPONSOR/MONITOR'S ACRONYM(S)

NASA

11. SPONSOR/MONITOR'S REPORT NUMBER(S)

NASA/CR-2012-217559

12. DISTRIBUTION/AVAILABILITY STATEMENT

Unclassified - Unlimited
Subject Category 02
Availability: NASA CASI (443) 757-5802

13. SUPPLEMENTARY NOTES

Langley Technical Monitor: James M. Luckring

14. ABSTRACT

A 14-percent-thick, slotted, natural-laminar-flow airfoil, the S204, for light business-jet applications has been designed and analyzed theoretically. The two primary objectives of high maximum lift, relatively insensitive to roughness, and low profile drag have been achieved. The drag-divergence Mach number is predicted to be greater than 0.70.

15. SUBJECT TERMS

aerodynamics; airfoils; laminar flow; wind tunnel experiment

16. SECURITY CLASSIFICATION OF:			17. LIMITATION OF ABSTRACT	18. NUMBER OF PAGES	19a. NAME OF RESPONSIBLE PERSON
a. REPORT	b. ABSTRACT	c. THIS PAGE			STI Help Desk (email: help@sti.nasa.gov)
					19b. TELEPHONE NUMBER *(Include area code)*
U	U	U	UU	68	(443) 757-5802